

# HIGH-RESOLUTION SIMULATIONS OF THE FINAL ASSEMBLY OF EARTH-LIKE PLANETS 1: TERRESTRIAL ACCRETION AND DYNAMICS

SEAN N. RAYMOND<sup>1,2</sup>, THOMAS QUINN<sup>1</sup>, & JONATHAN I. LUNINE<sup>3</sup>

*Draft version September 7, 2018*

## ABSTRACT

The final stage in the formation of terrestrial planets consists of the accumulation of  $\sim 1000$ -km “planetary embryos” and a swarm of billions of 1-10 km “planetesimals.” During this process, water-rich material is accreted by the terrestrial planets via impacts of water-rich bodies from beyond roughly 2.5 AU. We present results from five high-resolution dynamical simulations. These start from 1000-2000 embryos and planetesimals, roughly 5-10 times more particles than in previous simulations.

Each simulation formed 2-4 terrestrial planets with masses between 0.4 and 2.6 Earth masses. The eccentricities of most planets were  $\sim 0.05$ , lower than in previous simulations, but still higher than for Venus, Earth and Mars. Each planet accreted at least the Earth’s current water budget.

We demonstrate several new aspects of the accretion process: 1) The feeding zones of terrestrial planets change in time, widening and moving outward. Even in the presence of Jupiter, water-rich material from beyond 2.5 AU is not accreted for several millions of years. 2) Even in the absence of secular resonances, the asteroid belt is cleared of  $>99\%$  of its original mass by self-scattering of bodies into resonances with Jupiter. 3) If planetary embryos form relatively slowly, following the models of Kokubo & Ida, then the formation of embryos in the asteroid belt may have been stunted by the presence of Jupiter. 4) Self-interacting planetesimals feel dynamical friction from other small bodies, which has important effects on the eccentricity evolution and outcome of a simulation.

*Subject headings:* planetary formation – extrasolar planets – cosmochemistry – exobiology

## 1. INTRODUCTION

The final stages of the formation of terrestrial planets consist of the agglomeration of a swarm of trillions of km-sized planetesimals into a few massive planets (see Lissauer, 1993, for a review). Two distinct stages in this process are usually envisioned: the formation of planetary embryos, and their subsequent accretion into full-sized terrestrial planets.

Runaway growth leads to the formation of Moon-to Mars-sized planetary embryos in the inner Solar System, in a process known as “oligarchic growth”. The total number of embryos is uncertain, and may range from  $\sim 30$ -50 if these are relatively massive to perhaps 500-1000 if embryos average only a lunar mass. The timescale for embryo formation is thought to increase with orbital radius, and decrease with the local surface density (Kokubo & Ida 2000, 2002). Thus, embryos form quickly at small orbital radii, and slower farther from the central star. Kokubo & Ida (2000) found that the timescale for embryo formation at 2.5 AU is roughly 10 million years. However, Goldreich *et al.* (2004) calculated a much shorter timescale for embryo formation in the inner disk,  $\sim 10^5$  years.

A jump in the local density may drastically reduce the timescale for embryo formation. Such a jump is expected immediately beyond the “snow line”, where the temperature drops below the condensation point of water (e.g., Stevenson & Lunine 1988). Beyond this jump, the isolation masses of embryos increase, yet their formation timescales decrease. These massive icy embryos are thought to be the building blocks of giant planet cores, following the “core-accretion” scenario for giant planet formation (Pollack *et al.* 1996). Thus, embryo formation is different interior to and exterior to the snow line – the longest

embryo formation timescales may lie in the *outer* regions of the *inner* disk (Kokubo & Ida 2002).

The stage of oligarchic growth is thought to end when roughly half of the total disk mass is in the form of embryos, and half in the form of planetesimals (Lissauer 1993). The final assembly of terrestrial planets consists of accretional growth of large bodies from this swarm, on timescales of about 50 million years (e.g., Wetherill 1996).

Several authors have simulated the late-stage accretion of terrestrial planets (e.g. Wetherill 1996; Agnor *et al.* 1999; Morbidelli *et al.* 2000; Chambers 2001; Raymond *et al.* 2004, 2005a, 2005b). Because of computational limitations, most simulations started from only  $\sim 20$ -200 particles. These simulations only included embryos in the terrestrial region, and could not probe the full mass range of embryos. In addition, they inevitably neglected the planetesimal component.

A significant physical process that requires a large number of bodies to model is dynamical friction. This is a damping force felt by a large body (e.g., a planetary embryo) in a swarm of smaller bodies (such as planetesimals). This effect certainly plays an important role in the final assembly of terrestrial planets (Goldreich *et al.*, 2004). Indeed, several sets of dynamical simulations have formed terrestrial planets with much higher orbital eccentricities and inclinations than those in the Solar System (Agnor *et al.* 1999; Chambers 2001; Raymond *et al.* 2004 – hereafter RQL04). Dynamical friction could possibly reconcile this discrepancy.

Here we present results of five high-resolution simulations, containing between 1000 and 2000 initial particles. For the first time, we can directly simulate a realistic number of embryos according to various models of their formation (see section 2).

<sup>1</sup>Department of Astronomy, University of Washington, Box 351580, Seattle, WA 98195 (raymond@astro.washington.edu)

<sup>2</sup>Current address: Laboratory for Atmospheric and Space Physics, University of Colorado, Boulder, CO 80309

<sup>3</sup>Lunar and Planetary Laboratory, The University of Arizona, Tucson, AZ 85287.

Our simulations are designed to examine the accretion and water delivery processes in more detail, and also to explore the dynamical effects of a larger number of particles. We focus our study on 1) the mass and 2) the orbital evolution of terrestrial planets. In addition to the accretion of terrestrial planets, we want to understand the source of their compositions, in particular their water contents and potential habitability. We address these issues in a companion paper (Raymond *et al.* 2006; hereafter Paper 2).

Section 2 discusses our initial conditions, i.e. our starting distributions of planetary embryos and planetesimals. Section 3 explains our numerical methods. Sections 4, 5, and 6 present the detailed evolution of each simulation. Section 7 concludes the paper.

## 2. INITIAL CONDITIONS

We choose three different sets of initial conditions for our high resolution simulations, shown in Figure 1 and summarized in Table 1. In all cases we follow an  $r^{-3/2}$  surface density profile with total mass in solid bodies between 8.5 and 10  $M_{\oplus}$ . All protoplanets are given small initial eccentricities ( $\leq 0.02$ ) and inclinations ( $\leq 1^{\circ}$ ). (Note that we use the term “protoplanets” to encompass both planetary embryos and planetesimals. This differs from certain previous uses of the term.)

The initial water content of protoplanets is designed to reproduce the water content of chondritic classes of meteorites (see Fig. 2 from RQL04): inside 2 AU bodies are initially dry; outside of 2.5 AU they have an initial water content of 5% by mass; and between 2 and 2.5 AU they contain 0.1% water by mass. The source of the water distribution in the Solar System is a combination of heating from the Sun (which determines the location of the snow line – e.g. Sasselov & Lecar 2002) and from radioactive nuclides, which may have been obtained from a nearby supernova early in the Sun’s history (Hester *et al.* 2004). These processes are complex and not fully understood; indeed, the location of the condensation point of water may not even track the innermost water-rich material (Cyr *et al.* 1998; Kornet *et al.* 2004). It is therefore unclear whether the Solar System’s initial water distribution is typical of protoplanetary disks in the Galaxy.

The starting iron contents of protoplanets are interpolated between the values for the planets (neglecting Mercury) and chondritic classes of meteorites, with values taken from Lodders & Fegley (1998), as in Raymond *et al.* (2005a, 2005b). To span our range of initial conditions, we extrapolate to values of 0.5 at 0.2 AU and 0.15 at 5 AU.

We begin simulation 0 in the late stages of oligarchic growth, when planetary embryos were not yet fully formed. The separation between embryos is randomly chosen to lie between 0.3 and 0.6 mutual Hill radii. The total number of protoplanets in the simulation is 1885, which is a factor of 5-10 more particles than previous simulations. The surface density at 1 AU is 10  $g\ cm^{-2}$ , and the total mass in embryos is 9.9  $M_{\oplus}$ , extending to 5 AU. A Jupiter-mass giant planet on a circular orbit is present at 5.5 AU.

In simulation 1, we follow the results of Kokubo & Ida (2000, 2002), who suggest that the timescale for the formation of planetary embryos is a function of heliocentric distance. Interior to the 3:1 resonance with Jupiter at 2.5 AU we include embryos. Exterior to the 3:1 resonance, we divide the total mass into 1000 “planetesimals” with masses of 0.006  $M_{\oplus}$ . We attempt to probe the dynamical effects of a swarm of planetesi-

imals, although these are still many orders of magnitude more massive than realistic planetesimals. The total mass in planetesimals and planetary embryos is 9.4  $M_{\oplus}$ , with roughly two thirds of the mass in planetesimals in the outer disk. The difference in total solid mass between simulations 0, 1 and 2 is not significant, and is simply the result of random spacing of bodies. Jupiter is included on a circular orbit at 5.2 AU – again, this is different than simulation 0, but not enough to cause a noticeable effect. We perform two simulations with the same initial conditions: a) In simulation 1a all bodies interact with each other, b) in simulation 1b the “planetesimals” past 2.5 AU are not self-interacting. They gravitationally interact with the embryos and Jupiter, but not with each other. This allows for significant computational speedup.

In Simulation 2, we assume that planetary embryos formed all the way out to 5 AU. However, a significant component of the total mass is still contained in a swarm of planetesimals which are littered throughout the region (between 0.5 and 5 AU). We include a total of 5.6  $M_{\oplus}$  in 54 embryos and 3  $M_{\oplus}$  in 1000 planetesimals, which are distributed with radial distance  $r$  as  $r^{-1/2}$  (the annular mass in our  $r^{-3/2}$  surface density profile). A Jupiter-mass giant planet is included at 5.2 AU on a circular orbit. As with simulation 1, we have run two cases – a) one in which planetesimals are treated in the same way as all massive bodies (simulation 2a) and b) one in which planetesimals do not interact with each other, but only with embryos and giant planets (simulation 2b).

Our three sets of initial conditions correspond to either different timescales for the formation of Jupiter, or different timescales for embryo formation. Jupiter is constrained to have formed in the few Myr lifetime of the gaseous component of the Solar Nebula (Briceño *et al.* 2001). According to Kokubo & Ida (2000, 2002), the timescale for planetary embryos to form out to 2.5 AU is  $\sim 10$  Myr, and even longer in the outer asteroid region (Goldreich *et al.* 2004 find a timescale of  $\sim 10^5$  years). Simulation 0 contains no embryo-sized bodies, and therefore represents a very fast timescale for Jupiter’s formation. Simulations 1a and 1b assume embryos to have formed out to 2.5 AU, and therefore represent a late formation for Jupiter (in the Kokubo & Ida model). Simulations 2a and 2b contain embryos out to 5 AU, and therefore represent either a very late formation time for Jupiter, or a much faster formation time for embryos. Previous simulations have generally assumed embryos to exist throughout the terrestrial zone, which is consistent with models predicting fast growth of embryos (Goldreich *et al.* 2004) but not with models predicting slower growth (Kokubo & Ida 2000, 2002).

The most important distinction between these and previous initial conditions is simply the scale: in the simulations from RQL04, planetary embryo masses ranged from about 0.03 to 0.2  $M_{\oplus}$ . In these simulations, we include bodies as small as  $10^{-3} M_{\oplus}$  (and some even less massive ones in the inner edge of simulation 0). The protoplanetary disks we are modeling are similar to previous simulations, but the number of particles is larger by roughly a factor of ten. As shown below, our increased resolution shows several new and interesting aspects of terrestrial accretion and water delivery.

## 3. NUMERICAL METHOD

In our simulations, we include roughly 5-10 times more particles than in previous simulations. The difficulty in including so many particles is that the number of operations

TABLE 1  
INITIAL CONDITIONS FOR 5 HIGH RESOLUTION SIMULATIONS

| Simulation | N(massive) <sup>1</sup> | N(non-int) <sup>2</sup> | $M_{TOT}(M_{\oplus})$ <sup>3</sup> | $a_{Jup}(AU)$ <sup>4</sup> |
|------------|-------------------------|-------------------------|------------------------------------|----------------------------|
| 0          | 1885                    | –                       | 9.9                                | 5.5                        |
| 1a         | 1038                    | –                       | 9.3                                | 5.2                        |
| 1b         | 38                      | 1000                    | 9.3                                | 5.2                        |
| 2a         | 1054                    | –                       | 8.6                                | 5.2                        |
| 2b         | 54                      | 1000                    | 8.6                                | 5.2                        |

<sup>1</sup>Number of massive, self-interacting particles.

<sup>2</sup>Number of non self-interacting particles.

<sup>3</sup>Total solid mass in planetary embryos and planetesimals.

<sup>4</sup>Orbital radius of Jupiter-mass giant planet.

scales strongly with the number of particles  $N$ . The computational time required for serial algorithms such as `Mercury` (Chambers 1999) scales as  $N^2$ , whereas parallel codes such as `pkdgrav` (Stadel 2001) can improve the scaling to  $N \log(N)$ . One can overcome this issue in two ways: 1) simply allow simulations to run for a longer time with a serial code such as `Mercury`, or 2) use parallel machines to run alternative algorithms such as `pkdgrav` to speed up the calculations. Here we have followed (1), and simply run simulations for a longer time than before (we have also optimized `pkdgrav` for such calculations, which are in progress).

All simulations were evolved for at least 200 Myr, and were performed on 2.7 GHz desktop PCs using `Mercury` (Chambers 1999). Simulation 0 required 16 consecutive months of integration time. Simulation 1a and 2a took 4-5 months each. Simulations 1b and 2b took only 2-3 months of CPU time because most particles were not self-interacting, thereby greatly speeding up `Mercury`'s  $N^2$  force algorithm. We use a timestep of 6 days, to sample the innermost body in our simulation twenty times per orbit. Collisions are treated as inelastic mergers. Energy is conserved to better than 1 part in  $10^3$  in all cases.

#### 4. SIMULATION 0: 1885 INITIAL PARTICLES

Figure 2 shows six snapshots in time in the evolution of simulation 0. Embryos quickly become excited by their own mutual gravitation as well as that of the Jupiter-mass planet at 5.5 AU (not shown in plot). Objects in several distinct mean motion resonances have been excited by the 0.1 Myr snapshot and can be seen in Fig. 2: the 3:1 resonance at 2.64 AU, 2:1 resonance at 3.46 AU, and the 5:3 resonance at 3.91 AU. All material exterior to the 3:2 resonance at 4.2 AU is quickly removed from the system via collisions with and ejections by the giant planet, which we refer to as Jupiter, for simplicity. Once eccentricities are large enough for particles' orbits to cross, bodies begin to grow via accretionary collisions. This has started to happen in the inner disk by 1 Myr. These large bodies tend to have small eccentricities and inclinations, due to the dissipative effects of dynamical friction (equipartition of energy causes the smaller bodies to be more dynamically heated).

Accretion proceeds fastest in the the inner disk and moves outward, as can be seen by the presence of several large bodies inside 2 AU after 10 Myr. In the outer disk, collisions are much less frequent because of the slower dynamical timescales and decreasing density of material due to Jupiter clearing the region via ejections. However, the mean eccentricity of bodies in the outer disk is quite high, enabling those which are not

ejected by Jupiter to have their orbits move inward in time. After 30 Myr, the inner disk is composed primarily of a few large bodies, which have begun to accrete water-rich material from the outer disk. Larger bodies have started to form out to 2.5-3 AU, but their eccentricities are large. In time, several of these outer large bodies are incorporated into the three final terrestrial planets. We name the surviving planets *a*, *b*, and *c* (innermost to outermost). The properties of all the planets formed in our five high-resolution simulations are listed in Table 2. Plots like Fig. 2 of the evolution of each simulation are shown later in the paper.

#### 4.1. Mass Evolution of simulation 0 planets

In RQL04, the number of constituent particles that ended up in a given Earth-mass planet was typically 30-50. The three planets in simulation 0 formed from a much larger number of bodies: planet *a* (0.55 AU) from 500 protoplanets via 87 accretionary collisions, planet *b* (0.98 AU) from 457 protoplanets via 98 collisions, and planet *c* (1.93 AU) from 174 protoplanets via 47 collisions.

Figure 3 shows the “feeding zone” of each planet, the starting location of all bodies which were incorporated into that planet. Planet *a* contains 8% (5%) of material from past 2 AU (2.5 AU), planet *b* contains 25% (17%) from past 2 AU (2.5 AU), and planet *c* contains 37% (18%) from past 2 AU (2.5 AU). The feeding zone of planet *a* is much narrower than those of planets *b* and *c*, and is concentrated in the inner terrestrial zone. However, the feeding zones of the planets change in time.

Figure 4 shows the mass of each of the three final planets as a function of time. Planets *a* and *b* start to grow quickly, but planet *c* starts later because of the longer dynamical timescales in the outer terrestrial zone. We expect planet *a* to start growing faster than planet *b* for the same reason, but this is not the case. This is because the accretion seed of planet *b* originated very close to the seed of planet *a*, and was in the same region of rapid accretion at early times. Each planet grows quickly in the first few million years by accreting local material, but this rate flattens off within 20-30 million years. This happens fastest for planet *a* because the accretion in the inner disk is shortest, and most available material has been consumed within that time. The later stages of growth are characterized by a step-wise pattern representing a smaller number of larger-scale collisions with other “oligarchs”, which have also cleared out all bodies in their feeding zones. Such large, late impacts are reminiscent of the Moon-forming impact (e.g., Canup & Asphaug, 2001), which is thought to have occurred at low relative veloc-

TABLE 2  
 PROPERTIES OF (potentially habitable) PLANETS FORMED<sup>1</sup>

| Simulation           | Planet   | $a(\text{AU})$ | $\bar{e}^2$ | $\bar{i}(^{\circ})^3$ | $M(M_{\oplus})$ | W.M.F.                                 | N(oceans) <sup>4</sup> | Fe M.F.     |
|----------------------|----------|----------------|-------------|-----------------------|-----------------|--|------------------------|-------------|
| 0                    | a        | 0.55           | 0.05        | 2.8                   | 1.54            | $2.6 \times 10^{-3}$                   | 15                     | 0.32        |
|                      | <b>b</b> | <b>0.98</b>    | <b>0.04</b> | <b>2.4</b>            | <b>2.04</b>     | <b><math>8.4 \times 10^{-3}</math></b> | <b>66</b>              | <b>0.28</b> |
|                      | c        | 1.93           | 0.06        | 4.6                   | 0.95            | $9.1 \times 10^{-3}$                   | 33                     | 0.28        |
| 1a                   | a        | 0.58           | 0.05        | 2.7                   | 0.93            | $8.3 \times 10^{-3}$                   | 30                     | 0.31        |
|                      | <b>b</b> | <b>1.09</b>    | <b>0.07</b> | <b>4.1</b>            | <b>0.78</b>     | <b><math>5.5 \times 10^{-3}</math></b> | <b>17</b>              | <b>0.30</b> |
|                      | c        | 1.54           | 0.04        | 2.6                   | 1.62            | $1.2 \times 10^{-2}$                   | 75                     | 0.26        |
| 1b                   | a        | 0.52           | 0.06        | 8.9                   | 0.60            | $7.2 \times 10^{-3}$                   | 17                     | 0.31        |
|                      | <b>b</b> | <b>1.12</b>    | <b>0.05</b> | <b>3.5</b>            | <b>2.29</b>     | <b><math>6.7 \times 10^{-3}</math></b> | <b>60</b>              | <b>0.29</b> |
|                      | c        | 1.95           | 0.09        | 9.7                   | 0.41            | $3.8 \times 10^{-3}$                   | 6                      | 0.28        |
| 2a                   | a        | 0.55           | 0.08        | 2.6                   | 1.31            | $9.3 \times 10^{-4}$                   | 5                      | 0.33        |
|                      | <b>b</b> | <b>0.94</b>    | <b>0.13</b> | <b>3.4</b>            | <b>0.87</b>     | <b><math>8.6 \times 10^{-3}</math></b> | <b>29</b>              | <b>0.29</b> |
|                      | c        | <b>1.39</b>    | <b>0.11</b> | <b>2.4</b>            | <b>1.46</b>     | <b><math>6 \times 10^{-3}</math></b>   | <b>34</b>              | <b>0.29</b> |
| 2b                   | d        | 2.19           | 0.08        | 8.8                   | 1.08            | $1.8 \times 10^{-2}$                   | 75                     | 0.24        |
|                      | a        | 0.61           | 0.18        | 13.1                  | 2.60            | $7.1 \times 10^{-3}$                   | 71                     | 0.30        |
|                      | b        | 1.72           | 0.17        | 0.5                   | 1.63            | $2.0 \times 10^{-2}$                   | 126                    | 0.22        |
| Mercury <sup>5</sup> |          | 0.39           | 0.19        | 7.0                   | 0.06            | $1 \times 10^{-5}$                     | 0                      | 0.68        |
| Venus                |          | 0.72           | 0.03        | 3.4                   | 0.82            | $5 \times 10^{-4}$                     | 1.5                    | 0.33        |
| <b>Earth</b>         |          | <b>1.0</b>     | <b>0.03</b> | <b>0.0</b>            | <b>1.0</b>      | <b><math>1 \times 10^{-3}</math></b>   | <b>4</b>               | <b>0.34</b> |
| Mars                 |          | 1.52           | 0.08        | 1.9                   | 0.11            | $2 \times 10^{-4}$                     | 0.1                    | 0.29        |

<sup>1</sup> Planets are defined to be  $> 0.2M_{\oplus}$ . Shown in bold are bodies in the habitable zone, defined to be between 0.9 and 1.4 AU. This is slightly wider than the habitable zone of Kasting *et al.* (1993).

<sup>2</sup> Mean eccentricity averaged during the last 50 Myr of the simulation.

<sup>3</sup> Mean inclination averaged during the last 50 Myr of the simulation.

<sup>4</sup> Amount of planetary water in units of Earth oceans, where 1 ocean =  $1.5 \times 10^{24}$  ( $\approx 2.6 \times 10^{-4} M_{\oplus}$ ).

<sup>5</sup> Orbital values for the Solar system planets are 3 Myr averaged values from Quinn *et al.* (1991). Water contents are from Morbidelli *et al.* (2000). Iron values are from Lodders & Fegley (1998). The Earth's water content lies between 1 and 10 oceans – here we assume a value of 4 oceans. See text for discussion.

ity and an oblique impact angle.

There exists a constraint from measured Hf-W ratios that both the Moon and the Earth's core were formed by  $t \approx 30$  Myr (Kleine *et al.*, 2002; Yin *et al.*, 2002), suggesting that the Earth was at least 50% of its final mass by that time. Each of the three planets in simulation 0 reached half of its final mass within 10-20 Myr.

Figure 5 shows the bodies accreted by each of the surviving planets from simulation 0 (planet *a* in green, planet *b* in blue, planet *c* in red) as a function of time. The y axis represents the starting semimajor axis of each body, or in the case of objects which had accreted other bodies, the mass-weighted starting semimajor axis of the agglomeration. The relative sizes of accreted objects is also depicted. In the early stages of accretion, each planet accretes material from the inner disk, and the feeding zones of planets *a* and *b* overlap. In time, the planets clear their feeding zones of available bodies, and increase their mass and gravitational focusing factors.

Bodies in the outer terrestrial region and asteroid belt have their eccentricities pumped up via resonant excitation and secular forcing by Jupiter, as well as mutual close encounters. Many of these bodies are accreted by the planets. Until there exist large bodies with sufficient mass to scatter smaller bodies, eccentricities in a given region remain low and the region is dynamically isolated. The accretion of more distant bodies at later times reflects the dynamical change in these regions, from isolated groups composed of many small bodies to interacting groups dominated by a few large bodies. In effect, this change marks the end of oligarchic growth in a given region. The values from Fig. 5 are slightly longer than for simulations of oligarchic growth (Kokubo & Ida 2000). This is because we are

measuring the time for a body to grow and be accreted by planets at large distances rather than the formation time of planetary embryos, though the dynamical consequences are similar. For example, planets *a*, *b*, and *c* began accreting material from 2.5 AU and beyond after  $\sim 10$  Myr, as compared with a 10 Myr oligarchic growth timescale from Kokubo & Ida (2000).

Figure 5 shows that it is not until after about  $10^7$  years that water-rich bodies are accreted by the planets. At this late time, the feeding zones of all three planets are the same, and extend beyond the snow line. The vast majority of the water content of each planet originates between 2.5 and 4 AU. Material between 2-2.5 AU does not contain enough water, and the dynamical lifetimes of bodies past 3.5-4 AU are very short. This is discussed in more detail in Paper 2.

Figure 6 shows the mass of bodies accreted by each of the surviving planets from simulation 0 as a function of time. The size of each body is proportional to its mass<sup>1/3</sup>, and therefore represents its relative physical size. Bodies of a range of sizes are accreted by each planet throughout the simulation, although large impacts tend to happen later in the simulation. Some of these large impacts may form large satellites (moons). This is discussed in detail in Paper 2.

The radial time dependence of accretion seen in Fig. 5 is reflected in the positions of ejected bodies. Figure 7 shows the starting semimajor axes as a function of time of all bodies that were either ejected (blue) or accreted (red) by Jupiter. These bodies have had their eccentricities increased and had close encounters with Jupiter, which has either devoured them or scattered them from the system. During the first part of the simulation, only bodies past 4 AU are destroyed by Jupiter. But after  $\sim 10^7$  years, the initial location of ejected bodies is a scat-

ter plot, signaling the end of the isolation of accretion zones. Bodies from throughout the terrestrial region are scattered into interstellar space via close approaches to Jupiter.

In a disk of purely massless or non self-interacting particles, there would be no change in the trend like the one in Fig. 7 at  $10^7$  years. Rather, through secular forcing, bodies from the outer asteroid belt would have close encounters with Jupiter and be ejected. The zone cleared out by Jupiter would slowly widen in time, asymptotically reaching the point where the forced eccentricity could not induce a close enough approach to Jupiter. Additional zones would be cleared out via mean motion resonances. However, there would be no abrupt changes in the zones from which particles are ejected or accreted. This illustrates an important effect of the self-gravity of the protoplanetary disk.

#### 4.2. Eccentricity Evolution

Previous simulations of terrestrial accretion have not succeeded in reproducing the very low eccentricities of Earth, Mars, and Venus (Agnor *et al.* 1999; Chambers 2001; RQL04). The final eccentricities of the three planets at the end of the integration are 0.03, 0.09, and 0.07 for planets *a*, *b*, and *c*, respectively. However, these are instantaneous values not necessarily representative of the long-term evolution of the system. The mean eccentricities for planets *a*, *b*, and *c* from 100-200 Myr are 0.048, 0.039, and 0.057.

Figure 8 shows the eccentricity evolution of each planet from simulation 0 through time. During the first 20 Myr, while these planets were accreting material at a very high rate, their eccentricities remain relatively low, below 0.05-0.10. Collisions tend to circularize orbits, because they are most likely to happen when one body is at aphelion and the other at perihelion. In the period from 20-80 Myr, the planets' eccentricities increase and fluctuate wildly due to numerous close encounters with other massive bodies, which may increase eccentricities, but a slower rate of collisions. After this time, the planets' eccentricities are damped through interactions with the remaining small bodies in the system. The planets' eccentricities reach very low values at  $t \sim 150$  Myr. The mean eccentricities of the three planets from 150-170 Myr are 0.033 for planet *a*, 0.026 for planet *b*, and 0.057 for planet *c*.

At about 173 Myr, there is a jump in the eccentricities of the two inner planets, from about 0.03 to 0.05. This occurred due to the scattering of a Moon-sized ( $0.02 M_{\oplus}$ ) body from the asteroid belt into the inner terrestrial zone. Figure 9 shows the semimajor axes vs time of all surviving bodies for the last 50 Myr of the integration. Jupiter and the terrestrial planets are labeled by their final masses. Several bodies are ejected between 150-170 Myr, shown as vertical spikes as their semimajor axes increase to infinity. Beginning at  $t \approx 160$  Myr, two bodies in the asteroid belt begin to interact strongly and have several close encounters. At  $t = 173$  Myr, the smaller, roughly lunar-mass body is scattered by the larger, Mars-sized body into the terrestrial region. Its eccentricity is large enough that over the next twenty million years, this body has several close encounters with all three of the terrestrial planets, causing a large jump in their eccentricities. In time, the body is scattered outward and collides with Jupiter at  $t = 193$  Myr. Incidentally, the roughly Mars-mass scattering body is the largest object in the asteroid belt at this time, but is ejected from the system at  $t = 198$  Myr.

It is interesting to note in Fig. 8 how closely the eccentricity of the inner two planets track each other in time. Throughout the simulation, most sharp jumps are seen in the eccentricity

evolution of both bodies, and sometimes in the outer planet as well. By examining the planets' longitudes of perihelion, we have determined that planets *a* and *b* are in a secular resonance. Figure 10 shows a histogram of the relative orientation of the two planets' orbits. The relative orientation is measured by the quantity  $\Lambda$ , the difference in the two planets' longitudes of perihelion, normalized to lie between 0 and 180 degrees (Barnes & Quinn 2004). The sharp spike seen at  $\Lambda \approx 120^\circ$  with the tail to higher  $\Lambda$  values is the signature of secular resonance. It indicates that the orbits of planets *a* and *b* are librating about anti-alignment, with an amplitude of about  $60^\circ$ . The two planets' eccentricities are out of phase – planet *a*'s eccentricity is low when planet *b*'s is high, and vice versa. An interesting case from simulation 2a involving habitability will be discussed in section 8.

We explore two measures of the total dynamical excitement of the system as a function of time. The mass weighted eccentricity of all bodies is simply

$$MWE = \frac{\sum_j m_j e_j}{\sum_j m_j}, \quad (1)$$

where we sum over all surviving bodies *j* (excluding Jupiter). The angular momentum deficit measures the deviation of a set of orbits from perfect, coplanar circular orbits. This makes intuitive sense because the orbital angular momentum correlates roughly with the perihelion distance, so a circular orbit has the maximum angular momentum for a given semimajor axis. The angular momentum deficit includes both the inclination and eccentricity of bodies in its formulation, and is defined by Laskar (1997) as

$$S_d = \frac{\sum_j m_j \sqrt{a_j} (1 - \cos(i_j) \sqrt{1 - e_j^2})}{\sum_j m_j \sqrt{a_j}}, \quad (2)$$

where, in this case,  $i_j$  refers to a body's inclination with respect to the plane of Jupiter.

Figure 11 plots the mass-weighted eccentricity and angular momentum deficit of all bodies through the course of the simulation. The two measures of dynamical excitement track each other fairly well through the simulation, although the angular momentum deficit contains many more rapid fluctuations in time. This is because  $S_d$  is more sensitive than the  $MWE$  to small bodies, which may attain very high eccentricities and inclinations through close encounters. Each spike in  $S_d$  is due to a single, high-eccentricity (or high-inclination) particle which does not persist in this excited state. Rather, such a particle quickly falls into the Sun or is ejected from the system. For example, the four ejection events between 150-170 Myr seen in Fig. 9 can be correlated with small spikes in the angular momentum deficit in Fig. 11. Short term variations in the mass-weighted eccentricity are due to a combination of close encounters which pump up eccentricities, and destruction of high-*e* bodies via ejections or collisions, which decreases the mean eccentricity. In addition, both the mass weighted eccentricity and angular momentum deficit exhibit the jump at 173 Myr associated with the close encounter shown in Fig 9.

The mass weighted eccentricity of the four terrestrial planets in the Solar System and the largest asteroid, Ceres, is 0.037. The mean for the final 20 Myr of simulation 0 is 0.069, but for the low eccentricity period between 150 and 170 Myr, it is 0.046. The terrestrial planets in this simulation have significantly lower eccentricities than in most previous simulations

(e.g. Chambers 2001; RQL04). However, they are still larger than those in the Solar System.

Using 3 million year average values from Quinn *et al.* (1991), the angular momentum deficit of the Solar System terrestrial planets and Ceres is 0.0017, much smaller than  $S_d$  in Fig. 11. However, the value from simulation 0 is dominated by the few small bodies that remain in the asteroid belt on relatively high eccentricity and inclination orbits. If we restrict ourselves to only the three massive terrestrial planets, the value of  $S_d$  decreases sharply to roughly 0.0037 for the last 20 Myr of the simulation. In the period of very low eccentricities, from about 150-170 Myr,  $S_d$  averaged 0.0026, only 50% higher than for the recent, time-averaged Solar System. If we include only the terrestrial planets in the calculation, then  $S_d$  remains unchanged at 0.0017. However, if we include only Venus, Earth, and Mars,  $S_d$  drops to 0.0013. This indicates that the planets in simulation 0 are slightly more dynamically excited than the Solar System, but not by a large amount.

#### 4.3. Evolution of the asteroid belt

The evolution of orbits in the asteroid belt, defined to be exterior to 2.2 AU (roughly the 4:1 resonance with Jupiter), differs from that in the terrestrial region, as no large bodies remain after 200 Myr. The top panel of Figure 12 shows the most massive body in the asteroid belt from simulation 0 through time. Bodies up to  $0.26 M_{\oplus}$  may exist in the asteroid belt. However, these bodies are not able to survive in this region, and are removed by scattering from either Jupiter or other asteroid belt bodies. Many embryo-sized bodies did not accrete in the asteroid belt, but rather formed closer to the Sun and were scattered outward, where their eccentricities were damped causing them to remain on orbits in the asteroid belt. Accretion did take place in the asteroid region in simulation 0, but only to a limited extent. Nine bodies originating in the region reached masses of  $0.05 M_{\oplus}$ , and four reached  $0.1 M_{\oplus}$ . The most massive locally-formed body has  $0.2 M_{\oplus}$ . Accretion was primarily confined to the inner belt, as no bodies larger than  $0.1 M_{\oplus}$  formed past 3 AU.

Many previous authors (e.g. Agnor *et al.*, 1999; Morbidelli *et al.*, 2000; Chambers 2001) assumed that all of the mass in the asteroid belt was in the form of  $\geq$ Mars-sized planetary embryos. If these embryos form via oligarchic growth, separated by 5-10 mutual Hill radii, these would have masses in the asteroid belt between about  $0.08$  and  $0.17 M_{\oplus}$ . By starting our simulation from smaller bodies, we see that only a handful of such objects could actually form in the region on the relevant timescales (although we have not included the effects of very small bodies, which may be significant – Goldreich *et al.* 2004). Our results suggest that initial conditions containing embryos throughout the asteroid belt may not be realistic. This has important implications for the water delivery process, and is discussed in Paper 2.

The middle panel of Fig. 12 shows the evolution of the total mass in the asteroid belt. Our initial conditions included objects out to 5 AU. Virtually all particles exterior to the 3:2 Jupiter resonance at 4.2 AU were removed in the first few thousand years, causing the immediate steep drop from  $4.9 M_{\oplus}$  to  $4.2 M_{\oplus}$  in the first 10 thousand years. After the initial drop, mass is continuously lost from the asteroid belt. Most objects are either scattered into the terrestrial region to be incorporated into the terrestrial planets, or undergo a close encounter with Jupiter and are ejected from the system. The total mass ejected over the course of the simulation is  $3.08 M_{\oplus}$  out of  $9.9 M_{\oplus}$

of total solid mass. In addition,  $0.66 M_{\oplus}$  collided with Jupiter, and  $0.02 M_{\oplus}$  hit the Sun.

The asteroid belt is almost completely cleared of material, even though Jupiter is on a circular orbit. After 200 Myr, only five bodies remain in the asteroid belt, four of which are clustered around 3.1 AU (see Fig. 2), corresponding to the outer main belt in our Solar System, which is dominated by C-type asteroids. The total mass of these five surviving bodies in simulation 0's asteroid belt is  $0.07 M_{\oplus}$ , roughly 1.5% of the total mass. We continued the simulation to 1 Gyr, at which time only one  $0.03 M_{\oplus}$  body remained in the asteroid belt, comprising only 0.6% of the initial mass. Models of the primordial surface density of the asteroid belt suggest that the asteroid belt in our Solar System has been depleted by a factor of  $10^2 - 10^3$  (e.g., Weidenschilling 1977). Our results imply that such clearing is a natural byproduct of the evolution of the disk. As suggested by Morbidelli *et al.* (2000), the asteroid belt may be cleared simply by self-scattering of bodies onto unstable orbits such as resonances with Jupiter. We show that this can occur even with a very calm dynamical environment, with Jupiter on a circular orbit. In this situation, Jupiter's orbit does not precess (indeed, precession is meaningless with a circular orbit), so there are no secular resonances in the asteroid belt (such as the  $\nu_6$  resonance with Saturn at 2.1 AU). Tsiganis *et al.* (2005) suggest that the giant planets did not acquire appreciable eccentricities until about 600 Myr after the start of planet formation. Thus, even in this framework, the asteroid belt may have been rapidly cleared by the self-gravity of the disk.

The bottom panel of Fig. 12 shows the mass-weighted eccentricity through time of all bodies in the asteroid belt. A comparison with Fig. 11 shows that bodies in the asteroid belt have significantly higher eccentricities than those in the inner terrestrial region throughout the simulation. This is simply because bodies in the asteroid belt feel stronger perturbations than bodies closer to the Sun, due to Jupiter's proximity. In other words, the magnitude of the forced eccentricity for any particle in the asteroid belt is higher than for one in the terrestrial region. In time, the amplitude of short term oscillations in the *MWE* increases as the number of bodies decreases.

#### 5. SIMULATIONS 1A AND 1B: 1038 INITIAL PARTICLES

Simulations 1a and 1b both start with 38 planetary embryos to 2.5 AU, and 1000  $0.006 M_{\oplus}$  "planetesimals" between 2.5 and 5 AU (see Fig. 1). The starting positions of all embryos and planetesimals are identical in simulations 1a and 1b. The only difference between the two simulations is how planetesimals are treated. In simulation 1a, planetesimals are massive bodies which interact gravitationally with all other bodies in the simulation. In simulation 1b, however, planetesimals feel the gravitational presence of the embryos and Jupiter, but not each other's presence. In addition, these non-interacting planetesimals may not collide with each other. Any differences in the outcome of the two simulations therefore has to do with the properties of these particles.

The reasons for running a simulation which includes non self-interacting particles are several. Physically, we chose to run simulation 1b to test the importance of the self-gravity among small bodies in the protoplanetary disk (included in simulation 1a, but not in 1b). The effects are surprisingly important, as described below. In addition, the computational expense of including test particles is much less than for self-interacting particles, and scales with the number of particles  $N$  as  $N$  instead

of  $N^2$ . Therefore, many more such particles may be included in a simulation. However, the limitations of such simulations must be understood.

Figures 13 and 14 show six snapshots in the evolution of simulations 1a and 1b, respectively. One difference between the two simulations that is immediately evident is the shape of mean-motion resonances with Jupiter in the asteroid belt. In simulation 1a, the vertical structure of these resonances is washed out within 1 Myr, as resonant planetesimals excited by Jupiter excite other planetesimals in turn, and effectively spread out the resonance. In simulation 1b, however, the resonant structure is more confined and lasts longer, because of the lack of planetesimal-planetesimal encounters. The shape of the 3:2 resonance with Jupiter in simulation 1b is still intact after 1 Myr, and can be seen in Fig. 14. In both simulations, a swarm of surviving planetesimals appears to sweep into the terrestrial region at between 10 and 30 Myr, damping the eccentricities of large bodies. These planetesimals also deliver water to the surviving planets. In time, the numbers of planetesimals dwindle, but at different rates for the two simulations. This has important effects on the final eccentricities of the surviving planets, and is discussed below.

There are several similarities in the final planetary systems from simulations 1a and 1b. The positions of the two inner planets in each simulation are comparable (see Table 2 for details), although the masses of these planets differ significantly. The total mass in the three surviving planets from each simulation is nearly identical,  $3.3 M_{\oplus}$ . The total water content of these planets is also similar, although the planets in simulation 1a are slightly more water-rich, containing a total of 132 oceans of water as compared with 83 oceans contained in the planets of simulation 1b.

There exist significant differences between simulations 1a and 1b. Figure 15 shows the growth of the surviving terrestrial planets in simulations 1a (top panel) and 1b (bottom panel). It is clear that planets form faster in simulation 1a – they reach a significant fraction of their final mass at shorter times. In addition, the final large accretion event for each planet in simulation 1a occurs before  $t \approx 60$  Myr, while in simulation 1b this happens between roughly 70-90 Myr.

The main difference between the two simulations is the timing of the destruction of particles. Gravitational self-scattering of planetesimals in simulation 1a decreases the residence time of these bodies in the asteroid region compared with simulation 1b, and scatters them onto unstable orbits. Eventually, these bodies either have a close encounter with Jupiter and are ejected, or collide with a larger protoplanet. In addition, planetesimal collisions may occur, further decreasing the number of particles, although this effect is relatively minor.

The overall effects of this self-gravity are similar to those of the mass of asteroid region planetesimals explored in RQL04. In RQL04, we showed that more massive planetesimals cause the terrestrial planets to be more massive, more water-rich, to form more quickly, and to be fewer in number. Here we see that the self-gravity of planetesimals accelerates planet formation and moderately increases the water content of the terrestrial planets. The final planets from simulations 1a and 1b both contain roughly the same amount of mass. We can apply this to our result from RQL04, that a larger planetesimal mass causes the formation of a smaller number of more massive planets. That effect must be due to the amount of mass in the asteroid region in the “case (i)” simulations from RQL04, and not just dynam-

ical self-stirring.

The top panel of Figure 16 shows the evolution of the number of surviving particles in simulations 1a (blue) and 1b (red). The number of planetesimals drops much more rapidly in simulation 1a, and all are destroyed by  $t \approx 140$  Myr. The total mass in each simulation that either collides with Jupiter or is ejected is very similar, roughly  $6 M_{\oplus}$  of the  $9.3$  starting  $M_{\oplus}$ . Most of this is in the form of planetesimals, although some embryos are ejected. The evolution of the embryos is similar for the two cases. This is not surprising as embryos reflect the evolution of the inner disk, which starts with no planetesimals.

The bottom panel of Fig. 16 shows the mass-weighted eccentricity of all surviving particles from simulations 1a and 1b as a function of time. Eccentricities in both simulations grow rapidly at the start. Simulation 1b reaches higher eccentricities in the heavy accretion phase before 50 Myr. This is because planetesimals cannot damp their own eccentricities, which are elevated from a distance by secular and resonant perturbations from the embryos and Jupiter. In simulation 1a, collisions and dynamical stirring among planetesimals damp these eccentricities. In time, the eccentricities of both systems decrease, and flatten off at similar levels, with mass-weighted eccentricities of 0.05-0.07. Eccentricities are barely damped at all in either simulation after 100 Myr, as the number of total bodies has been reduced to just a few.

We may have run into a resolution limit, as no planetesimals remain at the end of simulation 1a or 1b. The only refuge of such bodies is the asteroid region, separated from both the terrestrial planets and Jupiter. The dynamical effects of small bodies on the planets are important in terms of damping eccentricities and inclinations. It is not clear from our simulations whether the vast majority of small bodies are necessarily destroyed within 200 Myr, meaning that even higher-resolution simulations are useless. A more complex treatment of terrestrial accretion could generate additional particles during each collision. This remains as an avenue for future study.

It is clear from the 10 Myr and 30 Myr panels of Figs. 13 and 14 that planetary embryos do exist in the asteroid region in both simulations 1a and 1b, even though the planetesimals in simulation 1b cannot accrete. These embryos did not form *in situ*, but were fully formed at the start of the simulation, interior to 2.5 AU, and were scattered into the asteroid belt in a process similar to “orbital repulsion” (Kokubo & Ida 1995). The embryos’ eccentricities were increased by gravitational stirring, and they were scattered beyond 2.5 AU. Dynamical friction acting on the large bodies damped their eccentricities without greatly altering their semimajor axes, thereby moving them out into the asteroid region. In this area, the orbits of embryos can be stable on 100 Myr timescales. Indeed, in simulation 1a, one embryo formed at 1.8 AU, quickly grew to  $0.35 M_{\oplus}$ , and was scattered into the asteroid region. It survived there for 200 Myr until being ejected at 211 Myr.

Few embryos formed in the asteroid belt in simulation 1a. Although accretion in the asteroid region did occur, only a handful of bodies accreted multiple other planetesimals, and only five accumulations contained four or more planetesimals. Indeed, the largest accumulation contained 8 planetesimals totaling only  $0.05 M_{\oplus}$ , comparable in size to the smallest embryos in the inner part of the disk. Embryos in the 2-2.5 AU region, separated by 5-10 mutual Hill radii, are typically  $0.1-0.2 M_{\oplus}$ . So, even the largest planetesimal accumulation was a factor of 2-3 smaller than its isolation mass. No large em-

bryos formed in the asteroid belt in simulation 1a, although a few embryos did form in the asteroid region in simulation 0, as discussed above. We conclude that accretion can happen in the asteroid belt, but only to a limited degree, forming a smaller number of less massive embryos than assumed in most previous accretion simulations (e.g. Morbidelli *et al.*, 2000).

## 6. SIMULATIONS 2A AND 2B: 1054 INITIAL PARTICLES

In simulations 1a and 1b we assumed that embryos formed only out to 2.5 AU, but in simulations 2a and 2b we assume that they formed all the way out to 5 AU. This corresponds to either a fast growth of embryos, as advocated by Goldreich *et al.* (2004), or perhaps a very slow growth of Jupiter. Simulations 2a and 2b have identical starting conditions (see Fig. 1), with 54 planetary embryos throughout the terrestrial region, embedded in a disk of 1000 “planetesimals” of  $0.003 M_{\oplus}$  each. Roughly two thirds of the mass is in the form of embryos, and one third in planetesimals. The only difference between simulations 2a and 2b is the way in which the planetesimals are treated: in simulation 2b the planetesimals do not feel each other’s presence, but in simulation 2a all particles are fully self-interacting.

Interestingly, the initial conditions for simulations 1a and 1b are reasonable if embryos form via the Goldreich *et al.* (2004) model, but are unrealistic if they follow the results of Kokubo & Ida (2000, 2002). The oligarchic growth phase is thought to end when the total mass in planetesimals and embryos is comparable (e.g., Lissauer 1993). Our initial conditions therefore represent a time after the completion of oligarchic growth. However, Kokubo & Ida’s model of oligarchic growth suggests that there may not be enough time for embryos to form in the outer terrestrial zone, in the asteroid region beyond 2-2.5 AU. Indeed, analysis of simulations 0 and 1a suggests that, if Jupiter was fully formed before embryos formed in the asteroid region, then perhaps five to ten embryos could have formed in this region. These would be sub-isolation mass objects, with masses of  $\sim 0.05 M_{\oplus}$  rather than the  $0.1 - 0.2 M_{\oplus}$  embryos in Fig. 1. In Kokubo & Ida (2000)’s model, embryos at 2.5 AU take roughly 10 Myr to form. The lifetime of gaseous disks around other stars is  $\leq 10$  Myr (Briceño *et al.* 2001), constraining the formation time of gas giant planets. Embryos form more slowly at larger orbital radii, so this model predicts that oligarchic growth in the asteroid region must have occurred in the presence of the giant planet, stunting the formation of embryos.

Figures 17 and 18 show snapshots in time of simulations 2a and 2b, respectively. The evolution of the two simulations is qualitatively similar in the first few Myr, but the outcomes are drastically different. Simulation 2a forms four terrestrial planets, including two in the habitable zone. Simulation 2b, in contrast, forms only two planets, one interior to and one exterior to the habitable zone.

Interactions among planetesimals appear to be very important to the dynamics of the system. The outcome of simulation 2b is very surprising in that the final terrestrial planets have very high eccentricities ( $e \sim 0.2$ ), not expected for a  $>1000$  particle simulation. Eccentricities in simulation 2a are slightly higher than in simulations 0, 1a and 1b, but are only about half of those in simulation 2b ( $e \sim 0.1$ ). The final angular momentum deficit of the planets in simulation 2a is one third of that for simulation 2b.

The early evolution of the simulations is not surprising – bodies are excited by resonances and mutual encounters. The

shapes of resonances are quickly washed out by the interactions among embryos. Dynamical friction between the embryos and planetesimals damps the eccentricities of the embryos and increases that of the planetesimals. This process appears to be stronger in simulation 2a than in simulation 2b. In each of the final three panels of Figs. 17 and 18, large bodies in simulation 2a have significantly smaller eccentricities than those in simulation 2b. The feeding zone of each planet is affected by its eccentricity; a larger eccentricity implies a larger radial variation during a body’s orbit, causing it to intercept more material than for a circular orbit (Levison & Agnor 2003). Indeed, the final planets in simulation 2b have high eccentricities and large masses.

Figures 19 and 20 show the time evolution of several aspects of simulations 2a and 2b, respectively. The top panels show the growth of the two final planets. The middle panels show the number of surviving bodies, both embryos and planetesimals, through time. The bottom panels show the mass-weighted eccentricity of all surviving bodies as a function of time. Note that the scale of the y axis for the bottom panels is different in the two figures.

The formation timescales are similar in simulations 2a and 2b. In both cases most accretion takes place in the first 30 Myr. The planets reach a significant fraction of their final masses by the end of rapid accretion. After this time, the planets accrete (often water-rich) planetesimals as well as possibly undergoing a large impact with another embryo.

In both simulations, the evolution of the mass-weighted eccentricity begins with the same rapid increase and bumpy profile seen in simulation 0 (Fig. 11). The eccentricities in simulation 1a in this early stage are slightly lower than those in simulation 2b. Eccentricities decrease in both simulations after  $t \approx 40$  Myr, after which their evolutions diverge. In both simulations, the decrease is followed by a sharp increase. However, the magnitude and duration of the increase are drastically different. In simulation 1a, the mass-weighted eccentricity reaches 0.2 at  $t = 50$  Myr, then begins a slow decline for the rest of the simulation. In simulation 2b, the eccentricity reaches values of almost 0.4 at  $t \approx 60$  Myr, and does not flatten out until 100 Myr. When it does flatten out, it does so at a much higher level than in the other simulations, about 0.2. The middle panel of Fig 20 shows that the increase in eccentricity at 50 Myr corresponds to the time when only a very few large bodies remain in the system, at the end of the rapid accretion phase. Indeed, only four embryo-sized bodies survive to  $t = 45$  Myr. As seen in the upper panel of Fig 20, two of these bodies are accreted by the surviving planets at 76 Myr and 127 Myr. However, the number of embryos at this time in simulation 2a is comparable. The differences lie in the evolution of the planetesimals.

During the time of very high eccentricities in simulation 2b, between roughly 50 and 100 Myr, only a few large bodies remain. Less than 100 planetesimals remain at the beginning of this period, and their destruction rate is accelerated at  $t \sim 50$  Myr, such that all are ejected by  $t \approx 75$  Myr. The increase in eccentricities is due to the lack of dissipative forces, i.e. no small bodies remain to provide dynamical friction. The same acceleration in the destruction rate of planetesimals is seen in simulation 1a at  $t \sim 55$  Myr. However, the curve flattens out, and several tens of planetesimals remain after the sharp increase in eccentricities at 50 Myr. Thus, large bodies in simulation 1a continue to feel dynamical friction, while those in simulation 1b do not.



Why do self-interacting planetesimals provide more dissipation than non self-interacting ones? In simulation 2a, eccentricities reached by the planetesimals are much smaller than in simulation 2b. This implies that interactions among planetesimals damp their eccentricities, i.e. planetesimals can feel dynamical friction from other planetesimals. By damping planetesimals' excitations, more are on low-inclination orbits likely to be encountered by embryos, increasing the damping. In addition, by staying on lower-excitation orbits, the lifetime of self-interacting planetesimals is longer. Unfortunately, the computational time needed to integrate the orbits of  $N$  self-interacting bodies scales as  $N^2$ , while non self-interacting bodies only scale as  $N$ .

It is interesting that self-interacting planetesimals survive longer in simulation 2a than simulation 2b, but non self-interacting planetesimals survive longer in simulation 1b than simulation 1a. In simulations 1a, planetesimals are primarily destroyed by ejection after being scattered by other planetesimals onto unstable resonances with Jupiter in the asteroid region. Non self-interacting particles in unstable resonances are cleared out quickly, but nearby orbits are not perturbed into instability. In contrast, the main destruction mechanism of planetesimals in simulations 2a and 2b is scattering by embryos onto unstable orbits. The eccentricities of non self-interacting planetesimals increase more rapidly than self-interacting planetesimals, so they are destroyed more quickly.

When all the planetesimals are destroyed, simulations proceed in the same fashion as previous, low resolution simulations which formed planets with relatively large eccentricities (e.g. Chambers 2001; RQL04). Secular perturbations and close encounters among the few remaining bodies excite their eccentricities. The feeding zones of these eccentric embryos are enlarged, and bodies are accreted until the system stabilizes with a small number of relatively massive, eccentric terrestrial planets. This occurs in simulation 2b, as planetesimals are destroyed before the end of accretion. In simulation 2a, however, some planetesimals survive through the end of accretion, keeping eccentricities low and planetary feeding zones narrow. The surviving planets in simulations 2a and 2b reflect this important difference in the evolution of their planetesimal populations.

A problem with our simulations is that the number of particles can only decrease. Realistic collisions between large bodies create a swarm of debris, the details of which depend on the collision velocity and angle (Agnor & Asphaug, 2004). Interactions between large bodies and this collisional debris tends to circularize the orbits of large bodies via dynamical friction (Goldreich *et al.* 2004). The reason for the high eccentricities in simulation 2b is the rapid destruction of all the small bodies. We included enough planetesimals to “resolve” the early parts of the simulation, but the planetesimals were all destroyed quickly. This problem may be solved in two ways, by either starting the simulation with even more particles than included here, by using self-interacting planetesimals (as in simulation 2a), or by creating debris particles during collisions. It would be very interesting to self-consistently create debris particles during oblique or high-velocity collisions, but this is left to future work.

## 7. CONCLUSIONS

We have run five simulations of terrestrial accretion with unprecedented resolution. The planets that formed were qualitatively similar to those formed in previous simulations, such as

RQL04. The mean eccentricities of our planets are smaller than in previous simulations, averaging about 0.05 vs. 0.1, but they remain larger than those of Venus, Earth, and Mars. This may be due to the resolution of our simulations, as the number of small bodies dwindles at late times. Perhaps a higher resolution simulation will further damp the terrestrial planet eccentricities. Future simulations may also include additional dissipative effects, such as accounting for dynamical friction from collisional debris.

We have uncovered several significant, previously unrecognized aspects of the accretion process:

1. The feeding zones of the terrestrial planets widen and move outward in time, as shown in Fig. 5. While the mass in a given annulus is dominated by small bodies, the damping effects effectively isolate that region by suppressing eccentricity growth. In time, large bodies form and material is scattered out of the region, ending its isolation period. The isolation time corresponds roughly to the oligarchic growth phase, and proceeds rapidly in the inner disk and moves outward in time. Assuming that embryos form slowly (as in Kokubo & Ida 2000), planets do not accrete water-rich material until at least 10 Myr after the start of a simulation, at which time most planets are a sizable fraction of their final mass.
2. The growth of planetary embryos in the asteroid belt may have been stunted by the presence of a giant planet. If embryos formed relatively slowly, following the results of Kokubo & Ida (2000), then perhaps ten or so smallish,  $\sim 0.05 M_{\oplus}$  embryos could form in the inner belt, out to about 3-3.5 AU. Beyond this, Jupiter's gravitational effects, as well as intrusion from embryos formed closer to the Sun, prevented their accretion. This result is independent of Jupiter's time of formation, because the 10 Myr timescale for embryos to form out to 2.5 AU (Kokubo & Ida 2000) corresponds to the upper limit on the formation time of Jupiter (Briceño *et al.* 2001). Embryos can form interior to 2.5 AU, be scattered into the asteroid belt and reside there for long periods of time, but are unlikely to form *in situ*. However, this result is model-dependent: Goldreich *et al.* (2004) calculate much shorter embryo formation timescales. In their model, embryos would certainly have formed before the giant planets, assuming these to form via core-accretion (Pollack *et al.* 1996) on a timescale of millions of years. The speed of embryo formation has important implications for the robustness of water delivery: if embryos form quickly, then the number of bodies involved in water delivery is relatively small, and the process is relatively stochastic (although less than in previous models – Morbidelli *et al.* 2004, RQL04).
3. Dynamical friction is a significant phenomenon for the growth of terrestrial planets. Indeed, even small bodies feel dynamical friction from a swarm of other small bodies. The high computational cost of fully-interacting simulations is therefore necessary to ensure a realistic outcome. The dynamics and outcome of simulations in which all particles interacted with each other were different than simulations in which our “planetesimals” were not self-interacting. Most severe was the case of simulations 2a and 2b. In simulation 2a, more planets formed than in simulation 2b (4 planets vs. 2) and the eccentricities of the final planets were far lower ( $e \approx 0.1$  vs.

$e \approx 0.2$ ). The lifetime of planetesimals was much longer in simulation 2a, because of dynamical friction due other small bodies. The consequences are important: the fraction of water delivered to terrestrial planets in the form of small bodies was twice as high in simulation 2a, and the timing of the delivery of water-rich embryos and planetesimals also varied among the two simulations.

4. The asteroid belt is cleared of >99% of its mass as a natural result of terrestrial accretion. Embryos and planetesimals scatter each other onto unstable orbits such as mean motion resonances with Jupiter. In time these bodies are

removed via ejections, or by colliding with bodies closer to the Sun. After  $\sim 1$  billion years, none of our simulations had more than 0.4% of their initial mass remaining in the asteroid belt. This result was also shown by Morbidelli *et al.* (2000) in the context of the current orbits of Jupiter and Saturn. In that case, many resonances exist in the asteroid belt, including the important  $\nu_6$  secular resonance with Saturn at 2.1 AU. Here we have shown that the asteroid belt is cleared even in a much calmer dynamical environment, with only one giant planet on a circular orbit.

#### REFERENCES

- Agnor, C. B., Canup, R. M., & Levison, H. F. 1999. On the Character and Consequences of Large Impacts in the Late Stage of Terrestrial Planet Formation. *Icarus*, 142, 219.
- Agnor, C., & Asphaug, E. 2004. Accretion Efficiency during Planetary Collisions. *ApJ*, 613, L157.
- Barnes, R. & Quinn, T., 2004. The (In)stability of Planetary Systems. *ApJ* 611, 494-516.
- Briceño, C., Vivas, A. K., Calvet, N., Hartmann, L., Pacheco, R., Herrera, D., Romero, L., Berlind, P., Sanchez, G., Snyder, J. A., Andrews, P., 2001. The CIDA-QUEST Large-Scale Survey of Orion OB1: Evidence for Rapid Disk Dissipation in a Dispersed Stellar Population. *Science* 291, 93-97.
- Canup, Robin M., Asphaug, Erik 2001. Origin of the Moon in a giant impact near the end of the Earth's formation. *Nature*, 412, 708-712.
- Chambers, J. E., 1999. A Hybrid Symplectic Integrator that Permits Close Encounters between Massive Bodies. *MNRAS*, 304, 793-799.
- Chambers, J. E. 2001. Making More Terrestrial Planets. *Icarus*, 152, 205-224.
- Chambers, J. E. & Cassen, P., 2002. The effects of nebula surface density profile and giant-planet eccentricities on planetary accretion in the inner Solar system. *Meteoritics and Planetary Science*, 37, 1523-1540.
- Cyr, K. E., Sears, W. D., & Lunine, J. I. 1998. Distribution and Evolution of Water Ice in the Solar Nebula: Implications for Solar System Body Formation. *Icarus*, 135, 537
- Drake, M. J. and Righter, K., 2002. What is the Earth made of? *Nature* 416, 39-44.
- Goldreich, P., Lithwick, Y., & Sari, R. 2004. Final Stages of Planet Formation. *ApJ*, 614, 497
- Gomes, R., Levison, H. F., Tsiganis, K., & Morbidelli, A. 2005. Origin of the cataclysmic Late Heavy Bombardment period of the terrestrial planets. *Nature*, 435, 466
- Hayashi, C. 1981. Structure of the solar nebula, growth and decay of magnetic fields and effects of magnetic and turbulent viscosities on the nebula. *Prog. Theor. Phys. Suppl.*, 70, 35-53.
- Hester, J. J., Desch, S. J., Healy, K. R., & Leshin, L. A. 2004. The Cradle of the Solar System. *Science*, 304, 1116
- Kasting, J. F., Whitmire, D. P., and Reynolds, R. T., 1993. Habitable zones around main sequence stars. *Icarus* 101, 108-128.
- Kleine, T., Munker, C., Mezger, K., Palme, H., 2002. Rapid accretion and early core formation on asteroids and the terrestrial planets from Hf-W chronometry. *Nature* 418, 952-955.
- Kokubo, E., & Ida, S. 1995. Orbital evolution of protoplanets embedded in a swarm of planetesimals. *Icarus*, 114, 247
- Kokubo, E. & Ida, S., 2000. Formation of Protoplanets from Planetesimals in the Solar Nebula. *Icarus* 143, 15-27.
- Kokubo, E. & Ida, S., 2002. Formation of Protoplanet Systems and Diversity of Planetary Systems. *ApJ* 581, 666.
- Kornet, K., Różycka, M., & Stepinski, T. F. 2004. An alternative look at the snowline in protoplanetary disks. *A&A*, 417, 151
- Laskar, J. 1997. Large scale chaos and the spacing of the inner planets. *A&A*, 317, L75
- Levison, H. F. & Agnor, C., 2003. The Role of Giant Planets in Terrestrial Planet Formation. *AJ*, 125, 2692-2713.
- Lissauer, J. J. 1993. Planet Formation. *ARAA*, 31, 129.
- Lissauer, J. J. 1999. How common are habitable planets? *Nature* 402, C11-C14.
- Lodders, K., & Fegley, B. 1998. The planetary scientist's companion. Oxford University Press, 1998.
- Morbidelli, A., Chambers, J., Lunine, J. I., Petit, J. M., Robert, F., Valsecchi, G. B., and Cyr, K. E., 2000. Source regions and timescales for the delivery of water on Earth. *Meteoritics and Planetary Science* 35, 1309-1320.
- Pollack, J. B., Hubickyj, O., Bodenheimer, P., Lissauer, J. J., Podolak, M., & Greenzweig, Y., 1996. Formation of the Giant Planets by Concurrent Accretion of Solids and Gas. *Icarus*, 124, 62-85.
- Quinn, Thomas R., Tremaine, Scott, & Duncan, Martin, 1991. A three million year integration of the earth's orbit. *AJ* 101, 2287-2305.
- Raymond, S. N., Quinn, T., & Lunine, J. I., 2004. (RQL04) Making other earths: dynamical simulations of terrestrial planet formation and water delivery. *Icarus*, 168, 1-17.
- Raymond, S. N., Quinn, T., & Lunine, J. I. 2005a. The formation and habitability of terrestrial planets in the presence of close-in giant planets. *Icarus*, 177, 256-263.
- Raymond, S. N., Quinn, T., & Lunine, J. I. 2005b. Terrestrial Planet Formation in Disks with Varying Surface Density Profiles. *ApJ*, 632, 670-676.
- Raymond, S. N., Quinn, T., & Lunine, J. I. 2006. (Paper 2) High-resolution simulations of the final assembly of Earth-like planets 2: water delivery and planetary habitability. *Astrobiology*, submitted, astro-ph/
- Regenauer-Lieb, K., Yuen, D. A., & Branlund, J. 2001. The initiation of subduction: Criticality by addition of water? *Science* 294(5542): 578-580.
- Sasselov, D. D. & Lecar, M. 2000. On the Snow Line in Dusty Protoplanetary Disks. *ApJ*, 528, 995
- Stevenson, D.J. & Lunine, J.I., 1988. Rapid formation of Jupiter by diffusive redistribution of water vapor in the solar nebula. *Icarus* 75, 146-155.
- Stadel, Joachim Gerhard 2001. Cosmological N-body simulations and their analysis. PhD Dissertation, University of Washington, Seattle.
- Tsiganis, K., Gomes, R., Morbidelli, A., & Levison, H. F. 2005. Origin of the orbital architecture of the giant planets of the Solar System. *Nature*, 435, 459
- Weidenschilling, S. J. 1977. The distribution of mass in the planetary system and solar nebula. *Ap&SS*, 51, 153
- Wetherill, G. W., 1996. The Formation and Habitability of Extra-Solar Planets. *Icarus*, 119, 219-238.
- Williams, D. M., Kasting, J. F., & Wade, R. A. 1997. Habitable moons around extrasolar giant planets. *Nature*, 385, 234-236.
- Williams, D. M., & Pollard, D. 2002. Extraordinary climates of Earth-like planets: three-dimensional climate simulations at extreme obliquity. *International Journal of Astrobiology*, 1, 1
- Yin, Qingzhu, Jacobsen, S. B., Yamashita, K., Blichert-Toft, J., Telouk, P., Albarede, F., 2002. A short timescale for terrestrial planet formation from Hf-W chronometry of meteorites. *Nature* 418, 949-952.

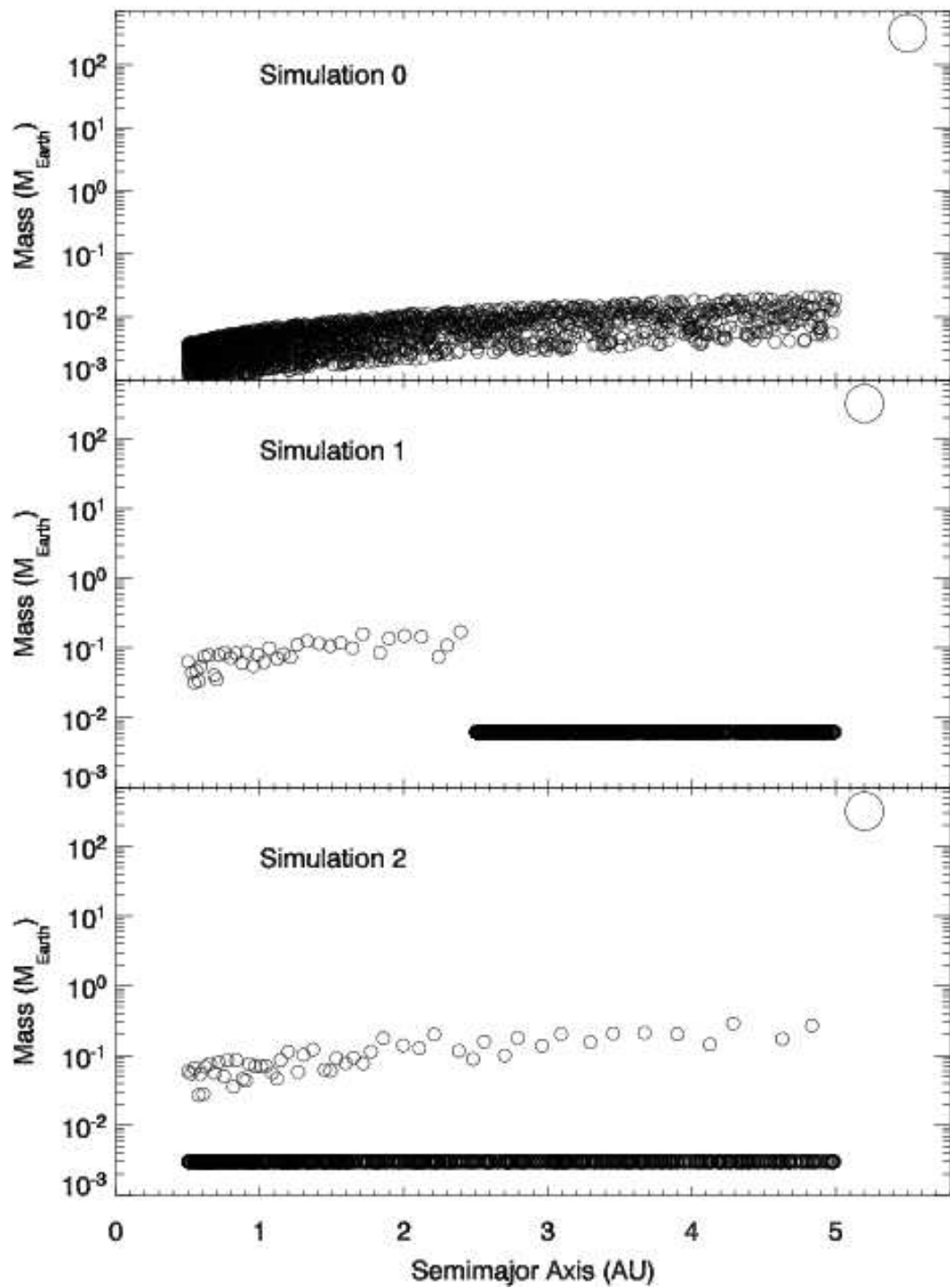


Fig. 1.— Our three sets of initial conditions for high-resolution simulations. The large circles at 5.5 and 5.2 AU are Jupiter-mass giant planets. The horizontal lines in simulations 1 and 2 represent 1000 planetesimals, which are distributed with orbital radius  $r$  as  $r^{-1/2}$ , corresponding to the annular mass in a disk with an  $r^{-3/2}$  surface density profile.

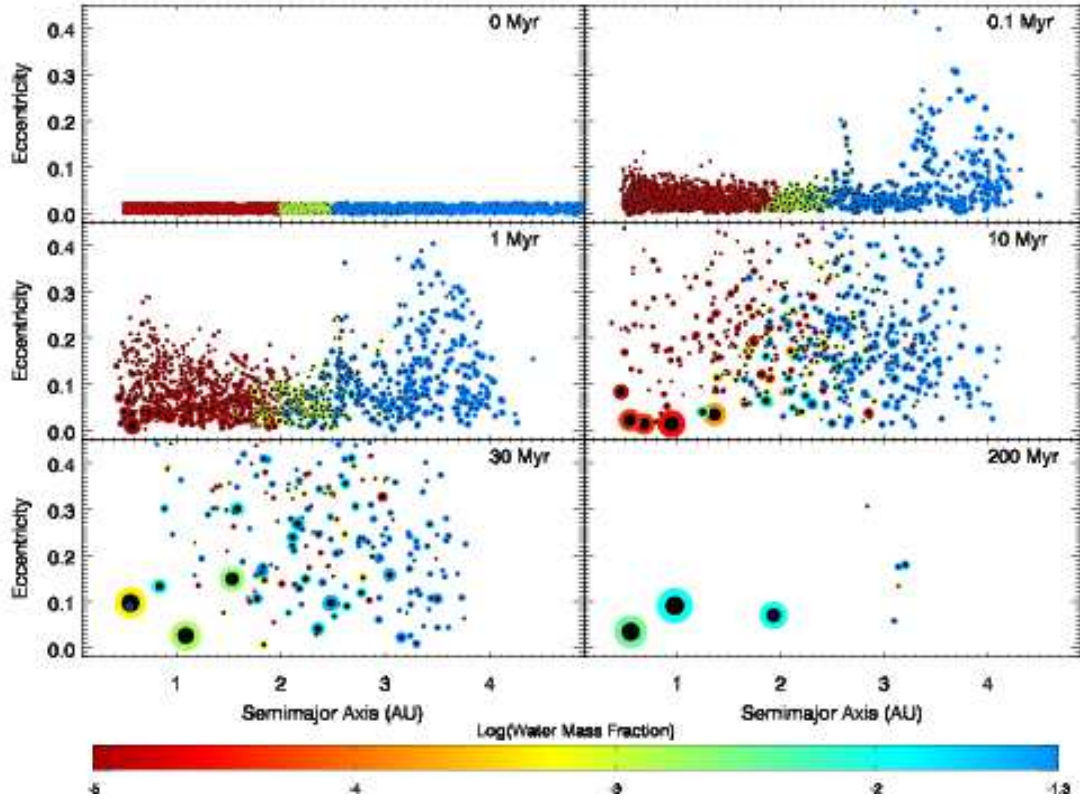


Fig. 2.— Six snapshots in time from simulation 0, with 1885 initial particles. The size of each body corresponds to its relative physical size (i.e. its mass  $M^{1/3}$ ), but is not to scale on the x axis. The color of each particle represents its water content, and the dark inner circle represents the relative size of its iron core. There is a Jupiter-mass planet at 5.5 AU on a circular orbit (not shown).

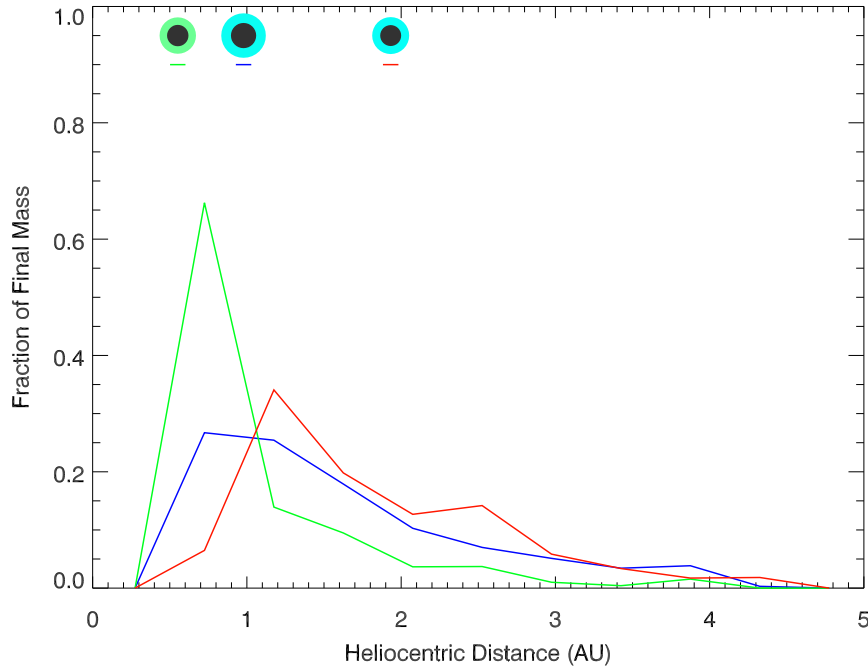


Fig. 3.— The feeding zones of the three surviving massive planets from simulation 0 (see Table 2). The y axis represent the fraction of each planet’s final mass that started the simulation in a given 0.45 AU wide bin. The final configuration of the planets is shown at top of the figure (as in the 200 Myr panel from Fig. 2). The color of each curve refers to the horizontal colored line below each planet.

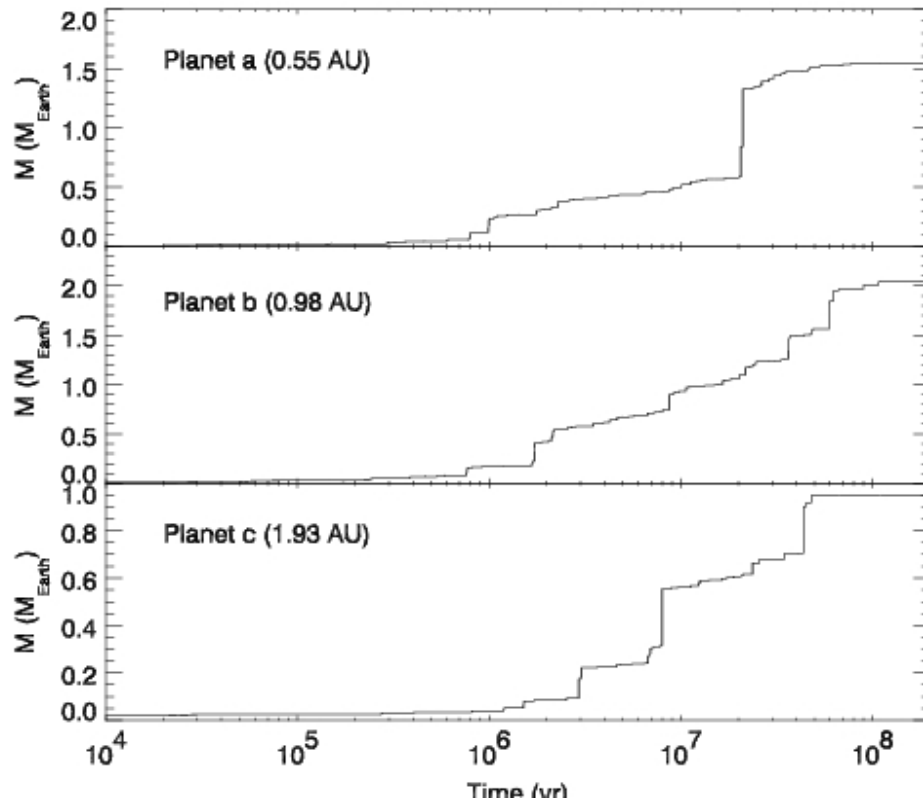


Fig. 4.— Mass vs time for the three surviving planets from simulation 0.

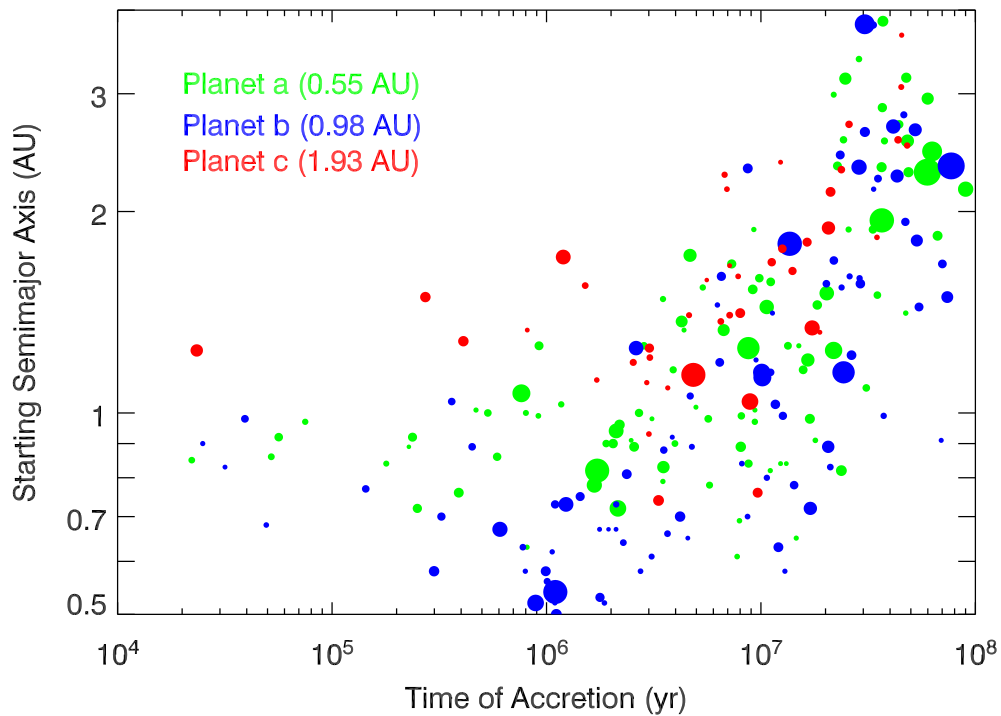


Fig. 5.— The timing of accretion of bodies from different initial locations for simulation 0. All bodies depicted in green were accreted by planet *a*, all blue bodies were accreted by planet *b*, and all red bodies were accreted by planet *c*. The relative size of each circle indicates its actual relative size. Impactors which had accreted other bodies are given their mass-weighted starting positions.

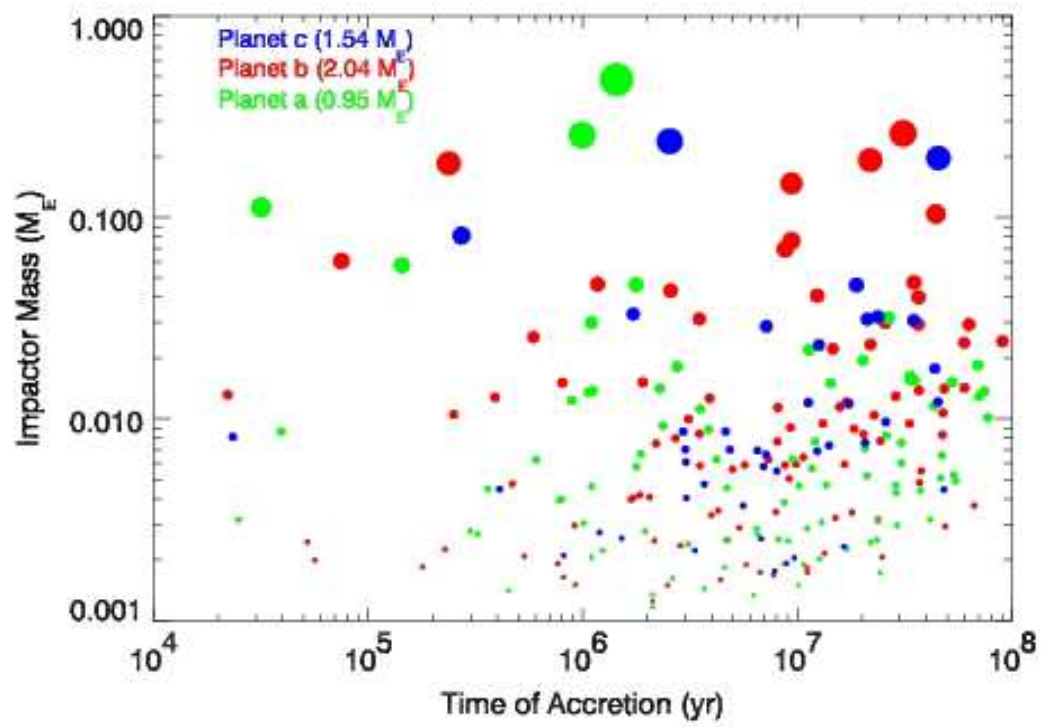


Fig. 6.— Impactor mass vs time for all bodies accreted by the surviving planets in simulation 0. As in Fig. 5, all bodies depicted in green were accreted by planet *a*, etc. The size of each body is proportional to its mass<sup>1/3</sup>, and represents its relative physical size.

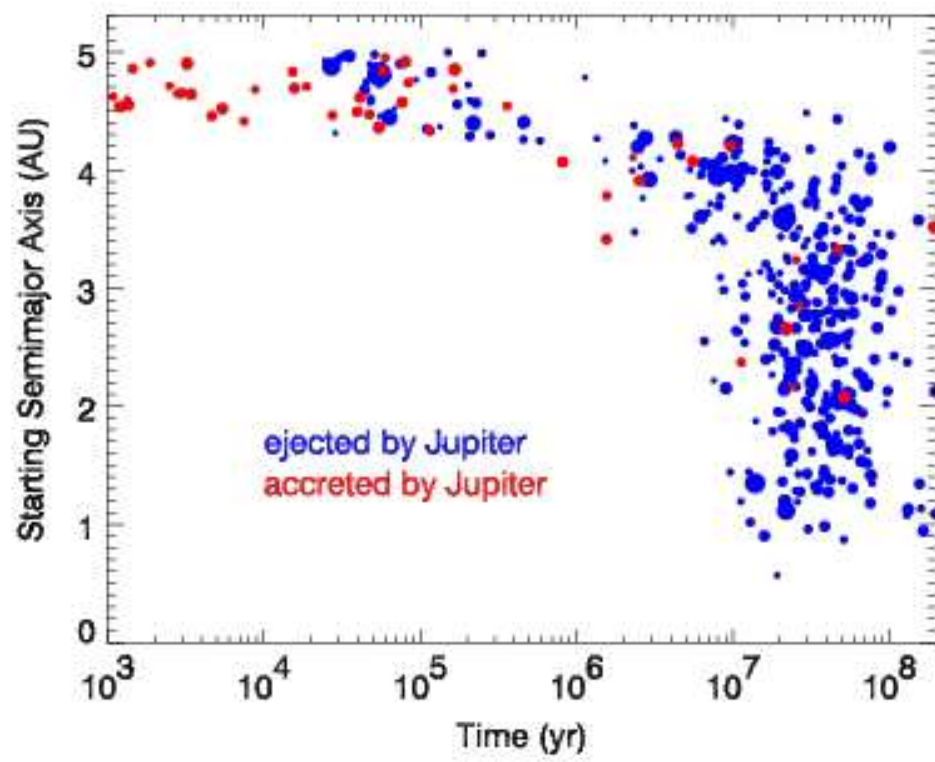


Fig. 7.— The timing of the ejection and accretion by Jupiter of bodies from different starting locations. Note the change in the “ejection zone” at  $t \approx 10\text{Myr}$ .

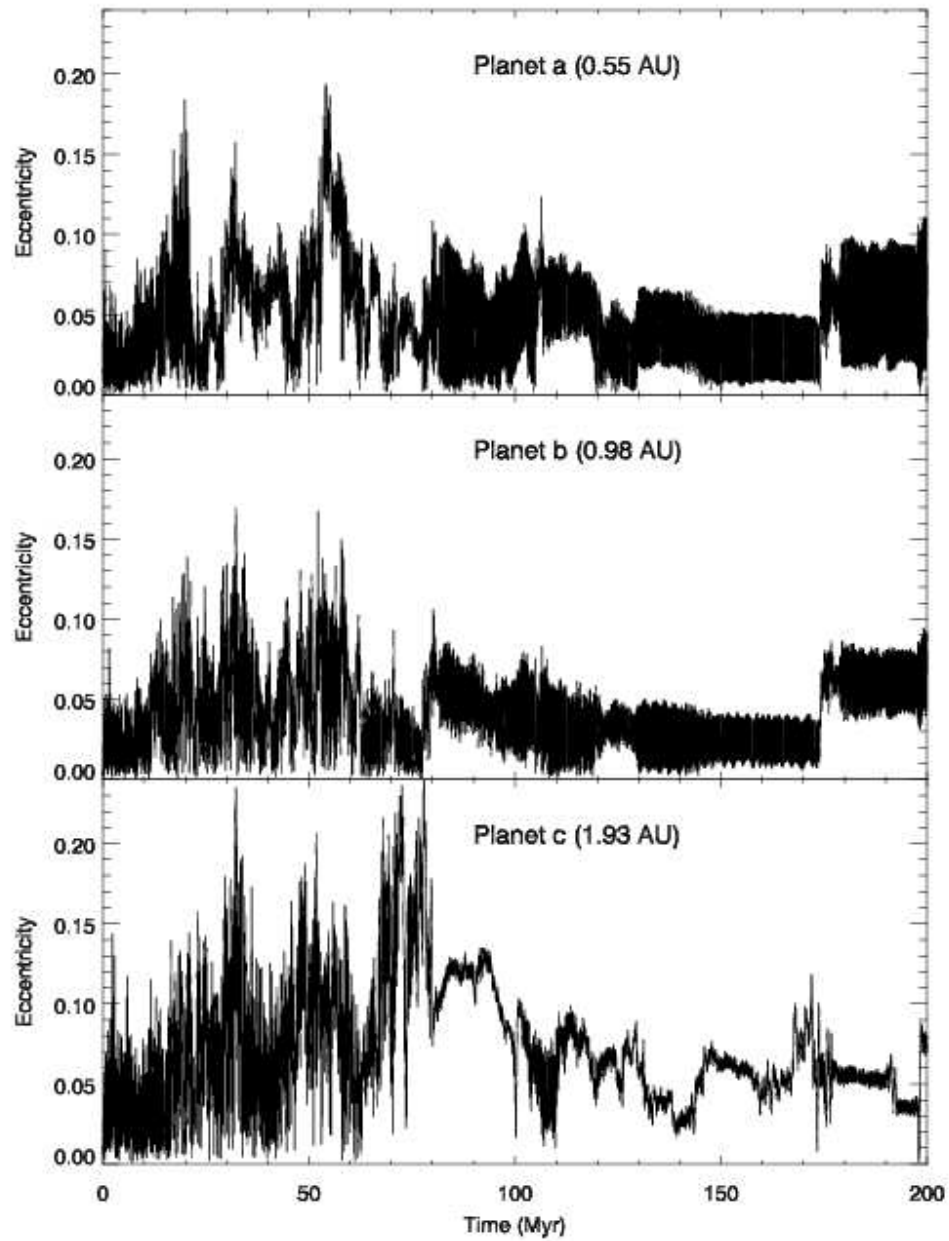


Fig. 8.— Eccentricity vs time for the three surviving massive planets. See Table 2 for details.



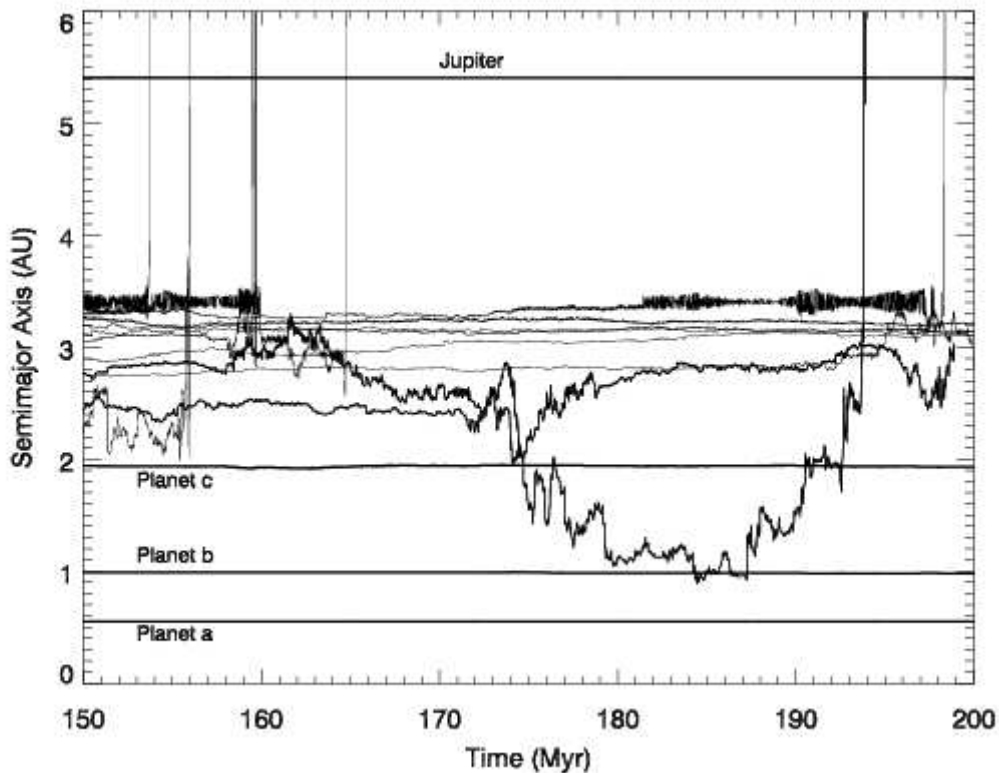


Fig. 9.— Semimajor axes of all bodies from simulation 0 for the time period from 150–200 Myr. The three surviving terrestrial planets and Jupiter are in bold and are labeled. Vertical spikes indicate a particle’s ejection from the system. Notice the encounter between a stray body and the terrestrial planets from about 173 to 193 Myr, which had a large effect on the eccentricities of the surviving planets (see Fig. 8). The body’s eccentricity was large enough ( $> 0.4$ ) that its orbit crossed that of planet *a*.

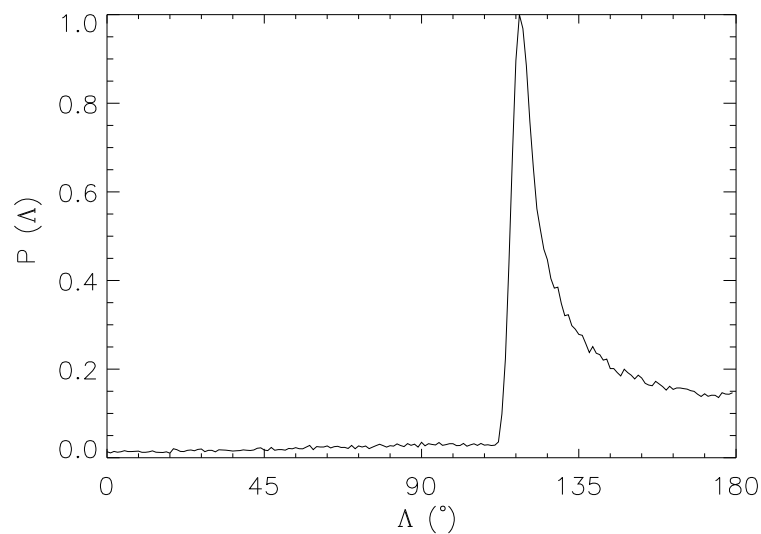


Fig. 10.— Normalized histogram of the relative orientation of the orbits of planets *a* and *b* from simulation 0 over one billion years.  $\Lambda$  represents the difference in the two planets’ longitudes of perihelion, normalized to lie between 0 and 180 degrees (Barnes & Quinn 2004). The spike at  $\Lambda \approx 120^\circ$  and tail to higher  $\Lambda$  values is reminiscent of a harmonic oscillator. It indicates that the two planets are locked in secular resonance, librating about anti-alignment with an amplitude of about 60 degrees.

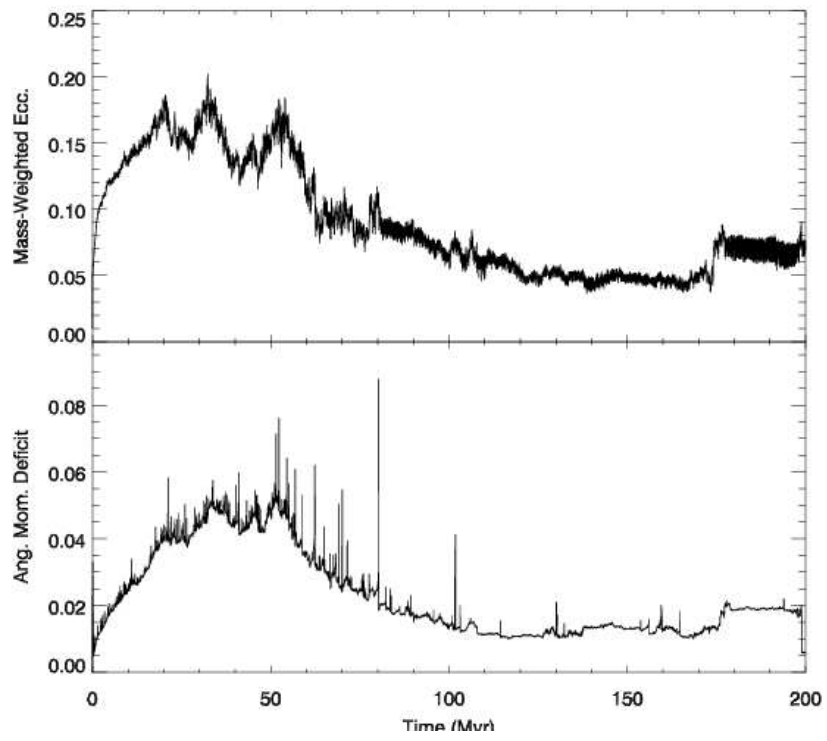


Fig. 11.— Top panel – Mass weighted eccentricity vs time for all bodies from simulation 0, excluding Jupiter. Bottom Panel – Angular momentum deficit vs time for all bodies from simulation 0, also excluding Jupiter. These quantities are defined in Eqs. 1 and 2.

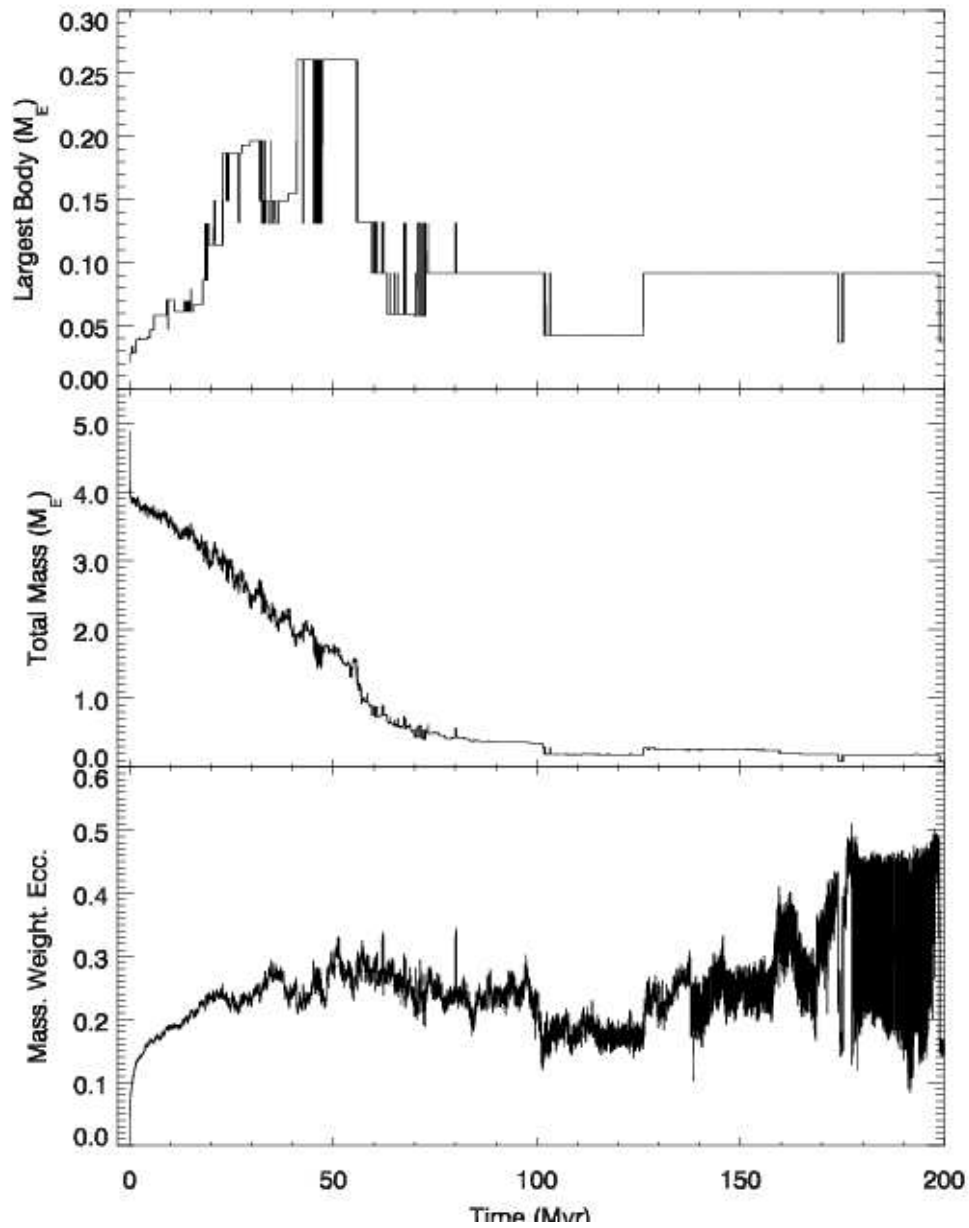


Fig. 12.— Evolution of the asteroid belt (defined as  $2.2 < a < 5.2$  AU) in time for simulation 0. Top – the most massive body in the asteroid belt through time. Middle – total mass in the asteroid belt as a function of time. Bottom – Mass-weighted eccentricity of all bodies in the asteroid belt over time.

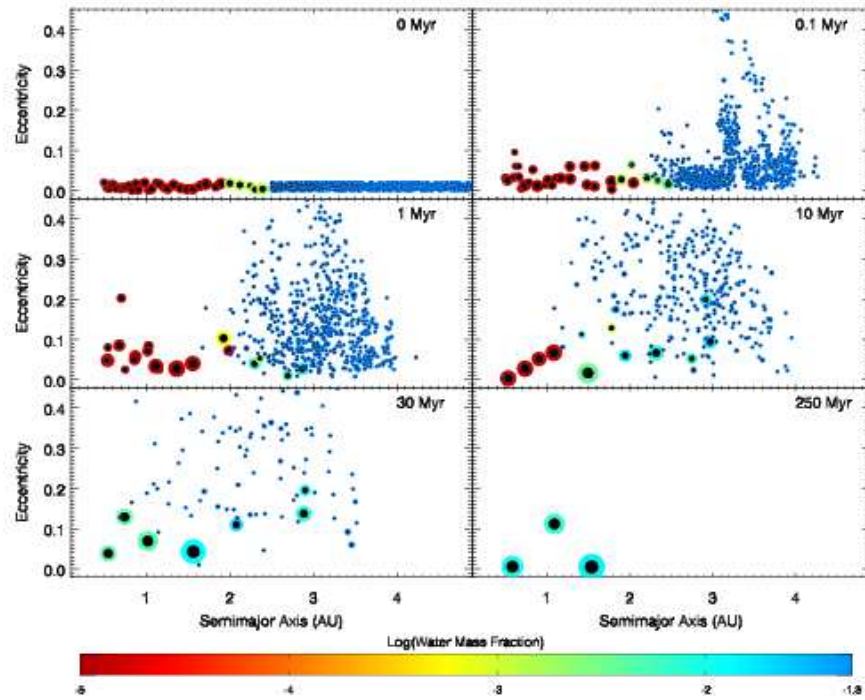


Fig. 13.— Six snapshots in the evolution of simulation 1a, with 1038 initial particles, all self-interacting.

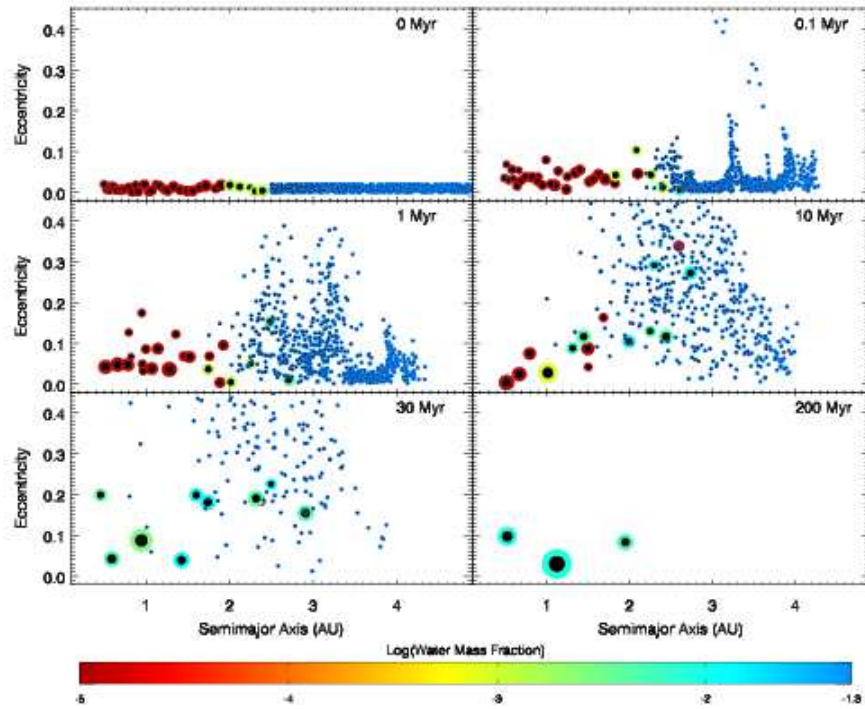


Fig. 14.— Six snapshots in the evolution of simulation 1b, with 1038 initial particles – 38 planetary embryos and 1000 non self-interacting planetesimals.

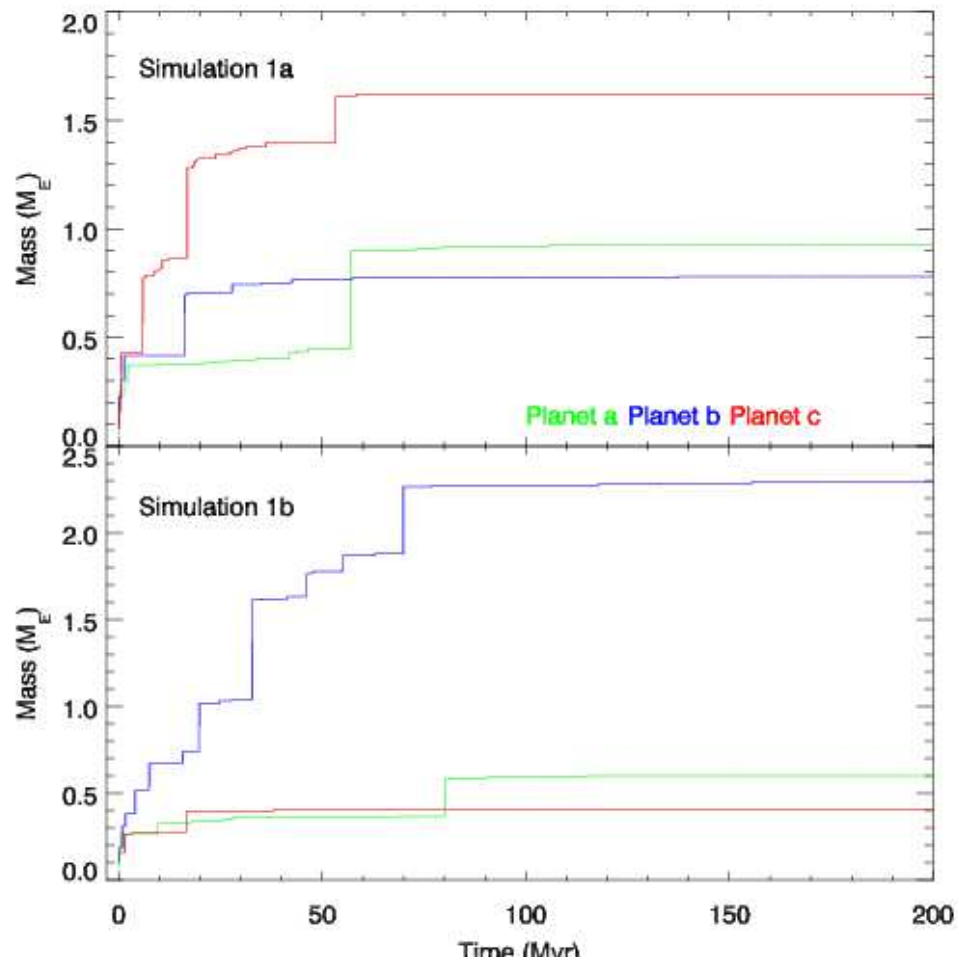


Fig. 15.— The masses of all surviving bodies from simulations 1a (top panel) and 1b (bottom panel) as a function of time. The innermost planet in each case (planet *a*) is shown in green, the middle planet (planet *b*) in blue, and the outer planet (planet *c*) in red.

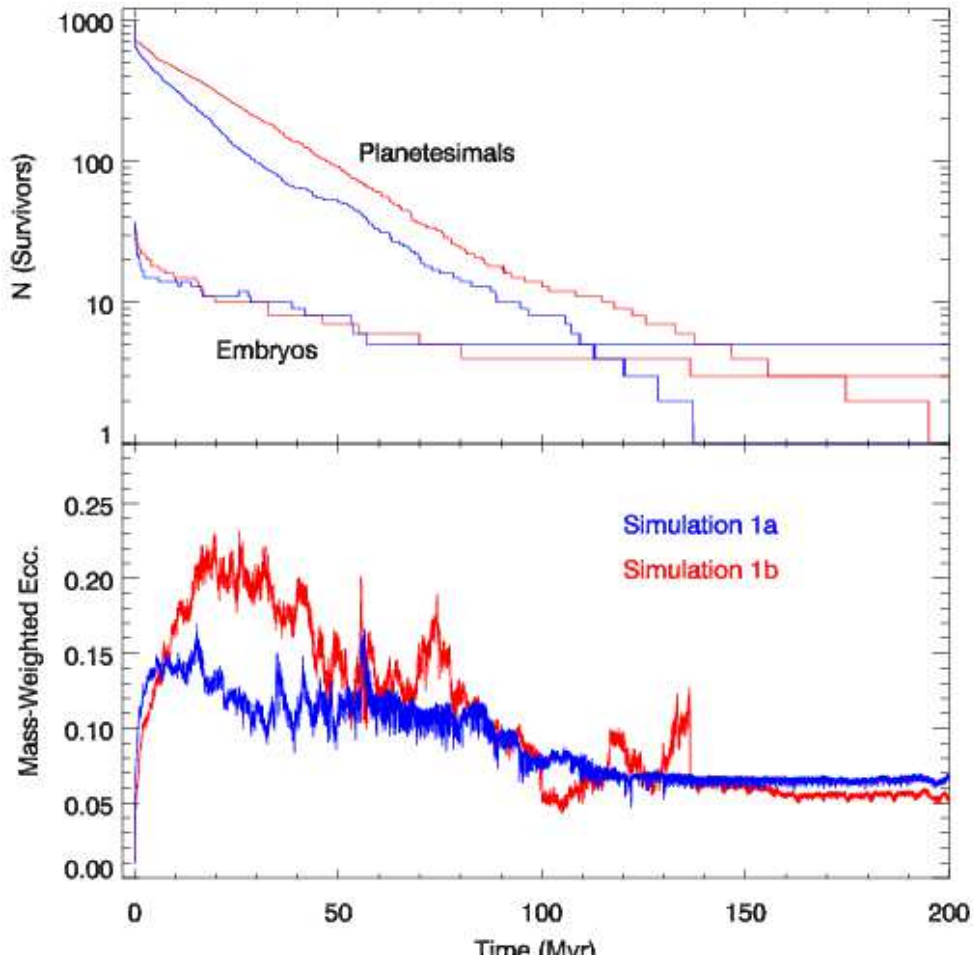


Fig. 16.— A comparison of the evolution of physical properties of simulations 1a (shown in blue) and 1b (red). Top: The number of surviving bodies, both planetesimals and planetary embryos. Bottom: The mass-weighted eccentricity of all surviving bodies.

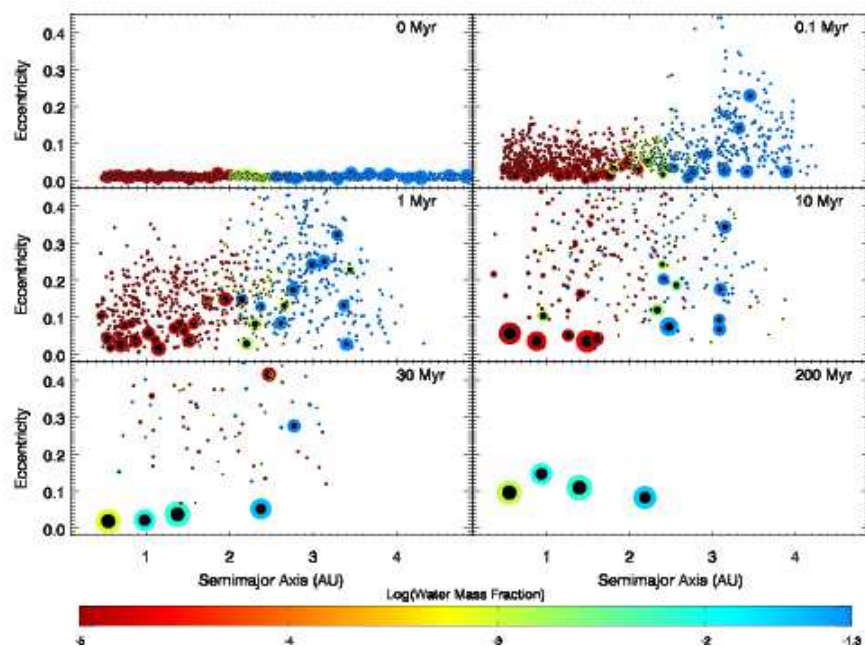


Fig. 17.— Six snapshots in the evolution of simulation 2a, with 1054 initial particles, all self-interacting.

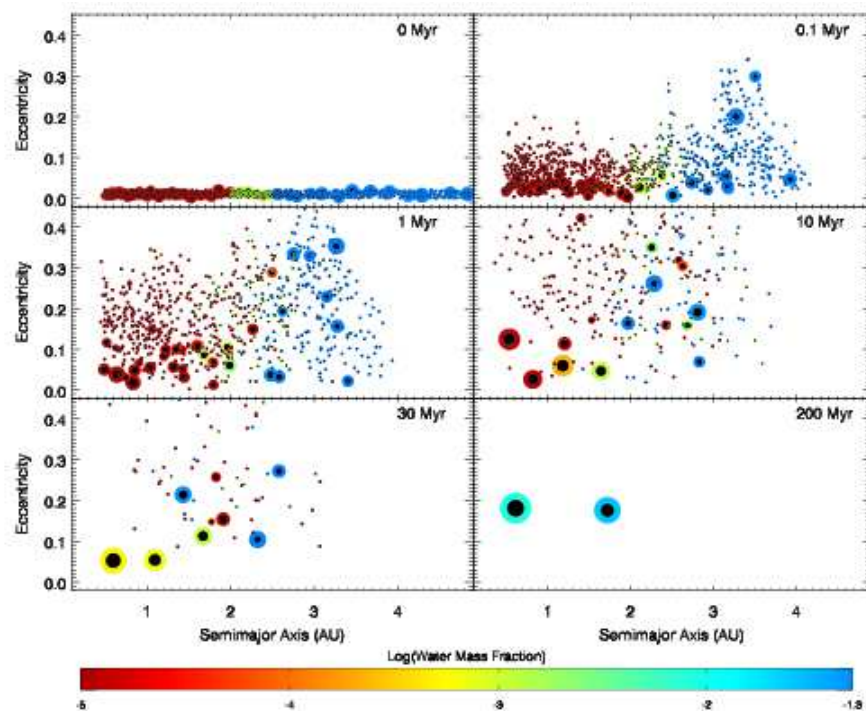


Fig. 18.— Six snapshots in the evolution of simulation 2b, with 1054 initial particles – 54 planetary embryos and 1000 non self-interacting planetesimals.

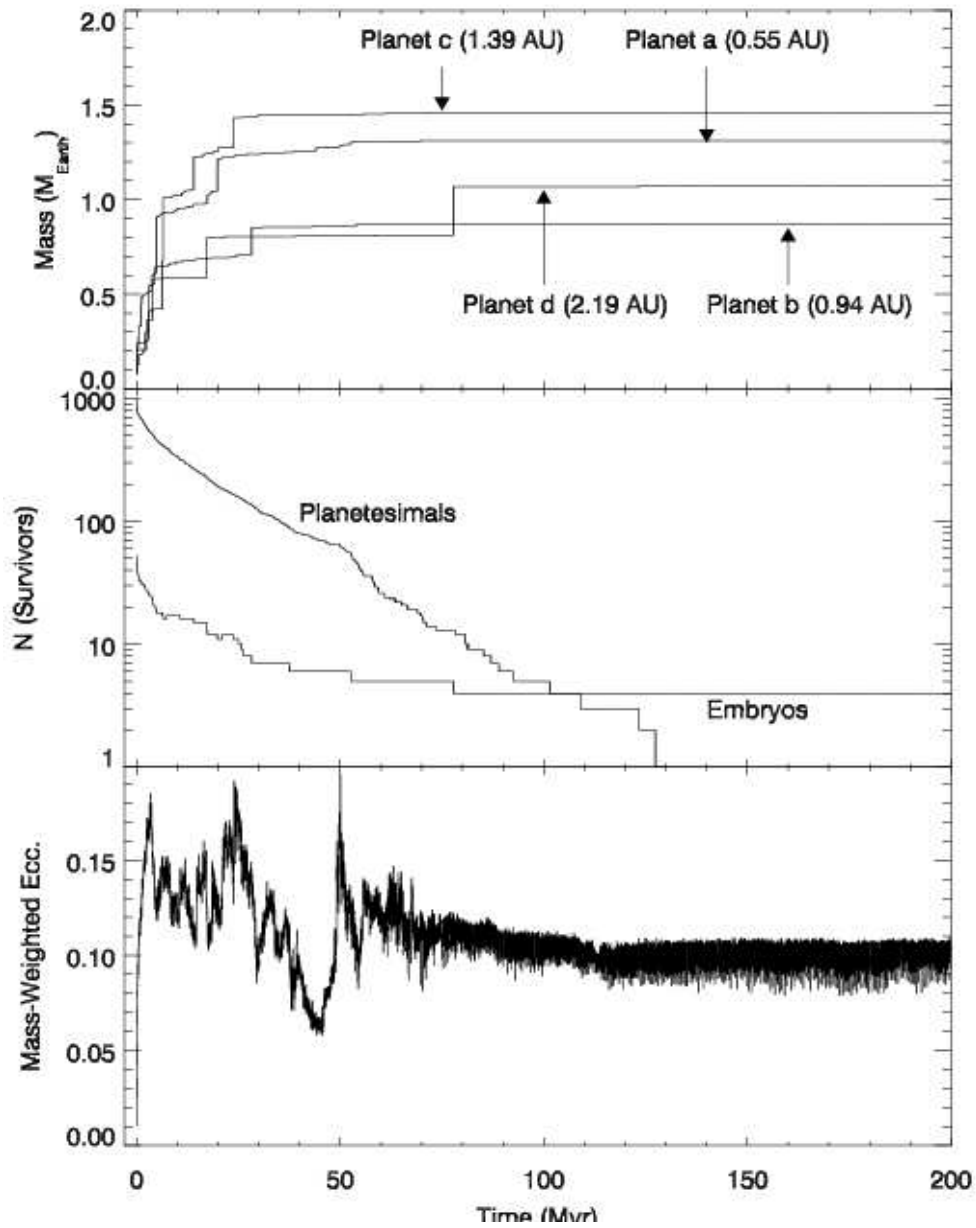


Fig. 19.— The evolution of simulation 2a. Top: Mass vs. time for the four surviving planets. Middle: Number of surviving planetary embryos through time. Bottom: Mass-weighted eccentricity as a function of time for all surviving bodies in the simulation (excluding Jupiter).



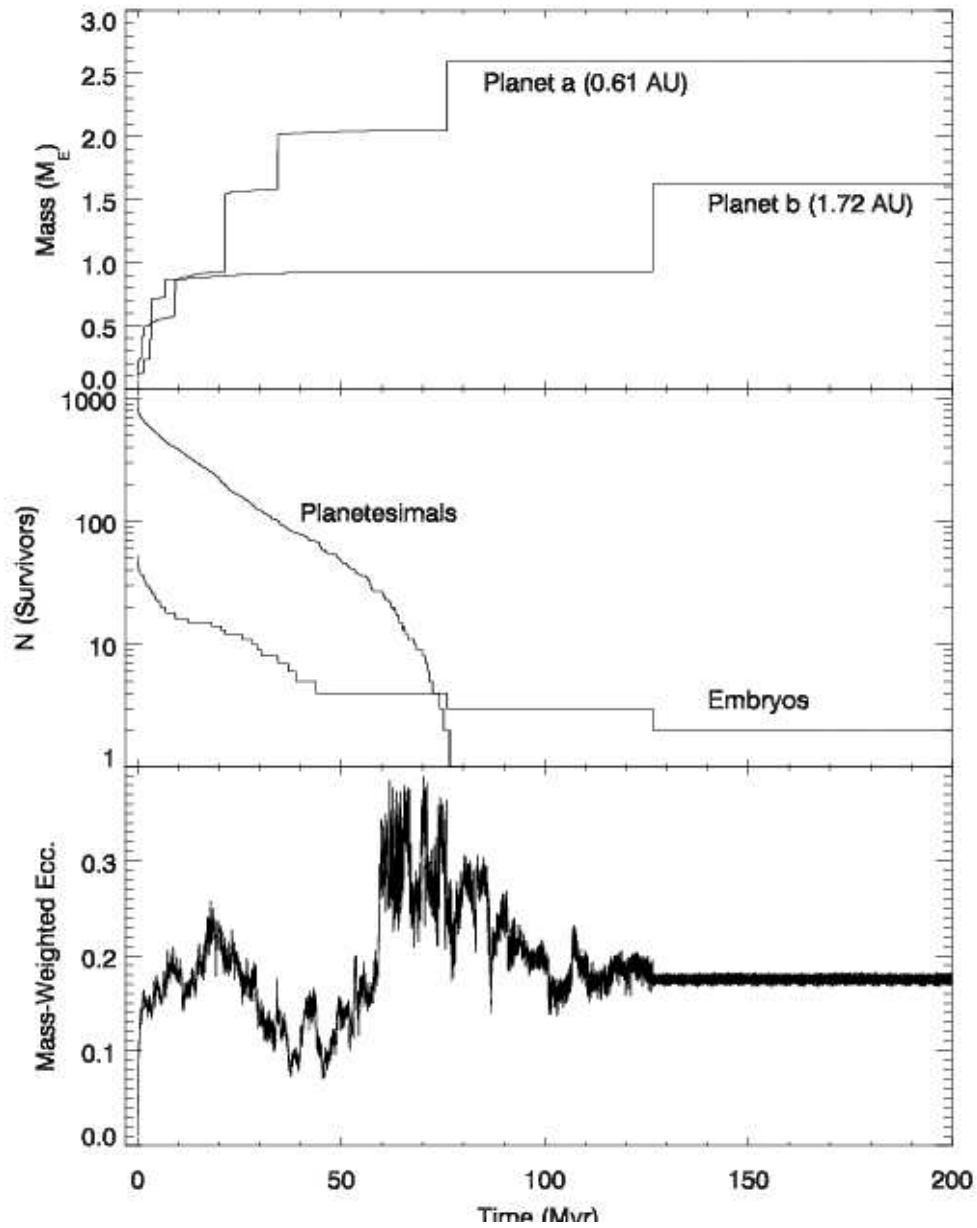


Fig. 20.— The evolution of simulation 2b. Top: Mass vs. time for the two surviving planets. Middle: Number of surviving planetary embryos through time. Bottom: Mass-weighted eccentricity as a function of time for all surviving bodies in the simulation (excluding Jupiter).